# Fault-controlled and stratabound dolostones in the Late Aptian-earliest Albian Benassal Formation (Maestrat Basin, E Spain): petrology and geochemistry constrains

Juan Diego Martín-Martín[1,2], Anna Travé[1], Enrique Gomez-Rivas[3], Ramón Salas[1], Jean-Pierre Sizun[4], Jaume Vergés[2], Mercè Corbella[5], Sherry Lynn Stafford[6], and Pura Alfonso[7]

[1]Departament de Geoquímica, Petrologia i Prospecció Geològica, Universitat de Barcelona, Martí i Franquès s/n, 08028 Barcelona, Spain
[2]Group of Dynamics of the Lithosphere (GDL), Institute of Earth Sciences Jaume Almera, ICTJA-CSIC, Lluís Solé i Sabarís s/n, 08028 Barcelona, Spain
[3]Department of Geology and Petroleum Geology, School of Geosciences, King's College, University of Aberdeen, Aberdeen AB24 3UE, UK
[4]UMR CNRS 6249 Chronoenvironment, Université de Franche-Comté, 16 Route de Gray, 25030 Besançon, France
[5]Departament de Geologia, Universitat Autònoma de Barcelona, 08193 Bellaterra, Spain
[6]ExxonMobil Upstream Research Company, 22777 Springwoods Village Parkway, Spring, TX 77389, USA
[7]Departament d'Ingenyeria de Minera i Recursos Naturals, Universitat Politècnica de Catalunya, Avd. Bases de Manresa, 08240 Manresa, Spain

Accepted 23 March 2015, Published online 31 March 2015

Published in **Marine and Petroleum Geology**, in press. doi:10.1016/j.marpetgeo.2015.03.019

**Abstract**

Fault-controlled hydrothermal dolomitization of the Late Aptian to Early Albian Benassal Fm shallow water carbonates resulted in the seismic-scale stratabound dolostone geobodies that characterize the Benicàssim case study (Maestrat Basin, E Spain). Petrological and geochemical data indicate that dolomite cement (DC1) filling intergranular porosity in grain-dominated facies constituted the initial stage of dolomitization. The bulk of the dolostone is formed by a replacive nonplanar-a to planar-s dolomite (RD1) crystal mosaic with very low porosity and characteristic retentive fabric. Neomorphic recrystallization of RD1 to form replacive dolomite RD2 occurred by successive dolomitizing fluid flow. The replacement sequence DC1-RD1-RD2 is characterized by a depletion in the oxygen isotopic composition (mean $\delta^{18}$O (V-PDB) values from -6.92, to -8.55, to -9.86‰), which is interpreted to result from progressively higher temperature fluids. Clear dolomite overgrowths (overdolomitization) precipitated during the last stage of the replacement. Strontium isotopic composition suggests that the most likely origin of magnesium was Cretaceous seawater-derived brines that were heated and enriched in radiogenic strontium and iron while circulating through the Paleozoic basement and/or Permo-Triassic red beds. Burial curves and analytical data indicate that the replacement took place at burial depths between 500 and 750 m, which correspond to the Late Cretaceous post-rift stage or early Tertiary extension of the Maestrat Basin, and by hydrothermal fluids likely exceeding temperatures of 80ºC. Following the partial dolomitization of the host rock, porosity considerably increased in dolostones by burial corrosion related to the circulation of acidic fluids likely derived from the emplacement of the Mississippi Valley-Type deposits. Acidic fluids, probably overpressured, circulated along faults, fractures and stylolites. Saddle dolomite and ore-stage calcite cement filled most of the newly created vuggy porosity. Subsequent to MVT mineralization, precipitation of calcite cements resulted from the migration of meteoric-derived fluids during uplift and subaerial exposure. This late calcite cement destroyed most of the dolostone porosity and constitutes the main cause for the present day poor reservoir quality of the Benassal Fm dolostones.

**Keywords:** dolostone; fault-controlled; hydrothermal; stratabound; fluid flow; Aptian

# 1 Introduction

Dolomitized limestone successions have been extensively studied during the last decades favored by the occurrence of important hydrocarbon reservoirs in dolostones. The key parameters controlling the distribution of rock heterogeneities in dolostones, which eventually control reservoir quality, are still poorly constrained, especially in those resulting from fault-controlled or fault-associated replacement processes (e.g. Duggan et al., 2001; Wilson et al., 2007; Sharp et al., 2010). Structurally-controlled dolostones commonly involve warm subsurface fluids, defining the so called hydrothermal dolomites (HTD) (Davies and Smith, 2006). These authors synthesized the most important characteristics of HTD in terms of fluid flow of dolomitizing brines along faults and fractures, and highlighted their close association with the genesis and location of Mississippi Valley-Type (MTV) mineral deposits.

Typically, dolostone geobodies adjacent to feeding faults (i.e. fault-related) are irregular in geometry and distributed in patches along the fault trace (e.g., Duggan et al., 2001; Wilson et al., 2007; López-Horgue et al., 2010; Shah et al., 2010; Sharp et al., 2010; Di Cuia et al., 2011; Lapponi et al., 2011; Dewit et al., 2012; Ronchi et al. 2012). Eventually, these bodies extend away from fault zones following suitable layers, resulting in a stratabound dolostone distribution (e.g., Sharp et al., 2010; Lapponi et al., 2011; Dewit et al., 2014). A Christmas tree-like morphology can be recognized when the replacement geometry includes both the patchy and the stratabound end members in an individual dolostone body (e.g., Sharp et al., 2010).

The formation of stratabound dolostones is commonly related to the circulation of dolomitizing fluids along most permeable beds, being grain-dominated carbonate facies typical preferential conduits (e.g., Davies and Smith, 2006; Wilson et al., 2007; Sharp et al., 2010). Lateral flow through permeability pathways like karstic units and/or aquitards are also claimed to facilitated the stratabound geometry (Sharp et al., 2010). More recently, the formation of stratabound HTD dolostones in Matienzo (Basque-Cantabrian Basin, Spain) has been related to mechanical stratigraphy, considering massive limestones beds major barriers to dolomitizing fluids (Dewit et al., 2014). Moreover, late authors claimed that depositional limestone facies played a minor role in the replacement process. Taken into account that mechanical stratigraphy represents the by-product of depositional composition, diagenetic evolution and structure (Laubach et al., 2009), new case studies of stratabound dolostones are of key interest in order to constrain major controls on the dolomitization process.

The Benicàssim outcrop analogue (Maestrat Basin, E Spain) constitutes a superb example of fault-controlled hydrothermal dolomitization that resulted in dominant stratabound dolostone geobody morphologies (Gomez-Rivas et al., 2010a, 2010b, 2014; Martín-Martín et al., 2010, 2013; Corbella et al., 2014). In Benicàssim, mud-dominated and highly stylolitized massive limestone beds appear unreplaced within the dolostones bodies, providing an opportunity to constrain the role of diverse parameters in the replacement. In this regard, the Late Aptian depositional facies of the Benicàssim host rock are similar to prolific hydrocarbon reservoirs in the Tethyan realm, and thus may represent a consistent analogue for age-equivalent carbonate reservoirs in the Middle East (Martín-Martín et al., 2013). In particular, the Benicàssim dolostones are of significant interest for the study of equivalent fault-controlled partially dolomitized hydrocarbon reservoirs worldwide, as well as those hydrocarbon reservoirs located offshore of eastern Spain (e.g., Clavell and Berastegui, 1991; Lomando et al., 1993).

This paper presents new petrographic and geochemical data of the Lower Cretaceous stratabound dolostones cropping out in the Benicàssim area. In particular, the aims of the study are: (i) to unravel the diagenetic evolution of the carbonate host rock with special emphasis on the replacement process; (ii) to constrain the composition and origin of the dolomitizing fluids; and (iii) to determine the controls on the development of stratabound morphology geobodies.

# 2 Geological setting

The Benicàssim area is located in the south of the Maestrat Basin (E Spain), which developed during the Late Jurassic-Early Cretaceous rift cycle of the Mesozoic Iberian rift system (Salas and Casas, 1993; Salas et al., 2001) (Fig. 1). The basin was inverted during the Alpine orogeny, and it is thus part of the intraplate Iberian Chain fold-and-thrust belt. Mesozoic syn-rift and contractive Alpine structures were subsequently reactivated and/or overprinted by an extensional phase during the Neogene period (Roca and Guimerà, 1992; Simón, 2004; Gomez-Rivas et al., 2012), which configured the present-day West Mediterranean basin (València Trough).

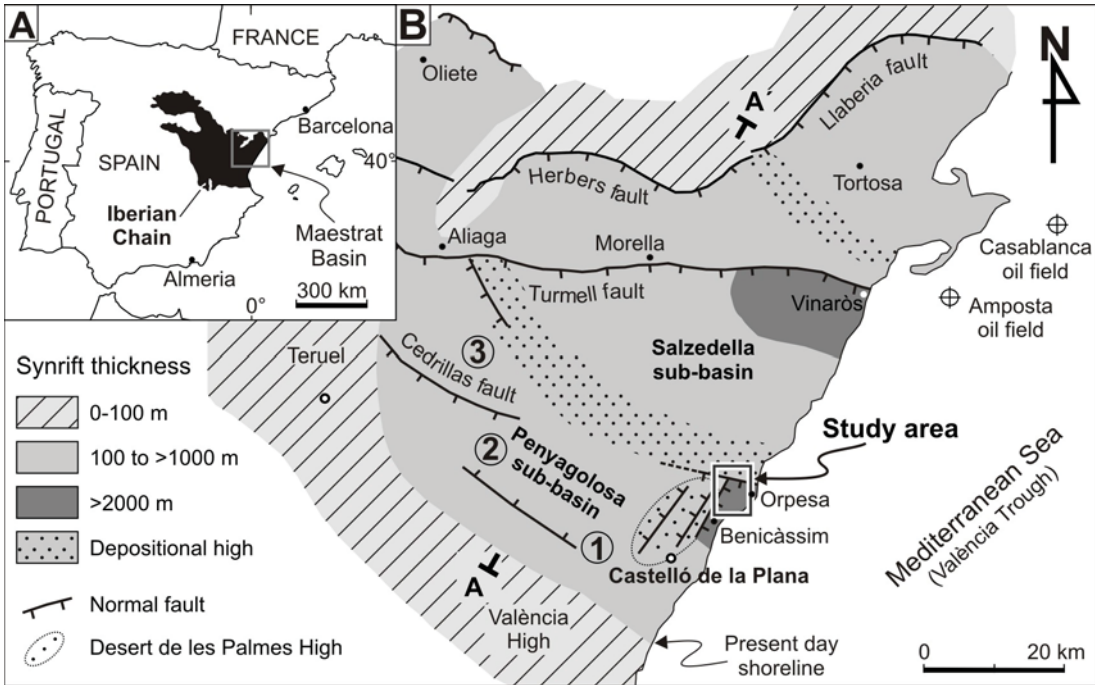


Figure 1: (A) Simplified map of the Iberian Peninsula showing the location of the Maestrat Basin. (B) Late Jurassic to Early Cretaceous paleogeographic map of the Maestrat Basin showing the thickness of syn-rift deposits (based on Salas et al., 2001). Besides Benicàssim, other occurrences of Lower Cretaceous dolostones hosting MVT deposits in the Penyagolosa sub-basin are labeled as: (1) Mas de la Mina; (2) Cedraman; and (3) Valdelinares. A and A refers to cross-section in figure 17.

During the Late Jurassic-Early Cretaceous, the regional NW-SE and NNE-SSW trending extensional faults of the Maestrat Basin resulted in the formation of rifted blocks that locally accommodated kilometer-thick Lower Cretaceous syn-rift deposits (Roca et al., 1994; Salas et al., 2001) (Fig. 1). In the study area, the intersection between the NW-SE-trending Campello fault and the NNE-SSW-trending Benicàssim fault resulted in the formation of a semi-graben structure that was filled with ∼2100-m-thick syn-rift deposits (Martín-Martín et al., 2013) (Figs. 1 and 2). These authors studied the syn-rift succession and reported one of the thickest Aptian sedimentary records from the western Tethyan realm. Moreover, the Lower Cretaceous syn-rift deposits appear partially dolomitized in close association with the aforementioned seismic-scale regional faults, providing a new case study of fault-controlled hydrothermal dolomitization. These dolostones locally host Mississippi Valley-type (MVT) ore deposits (Fig. 2 and 3).

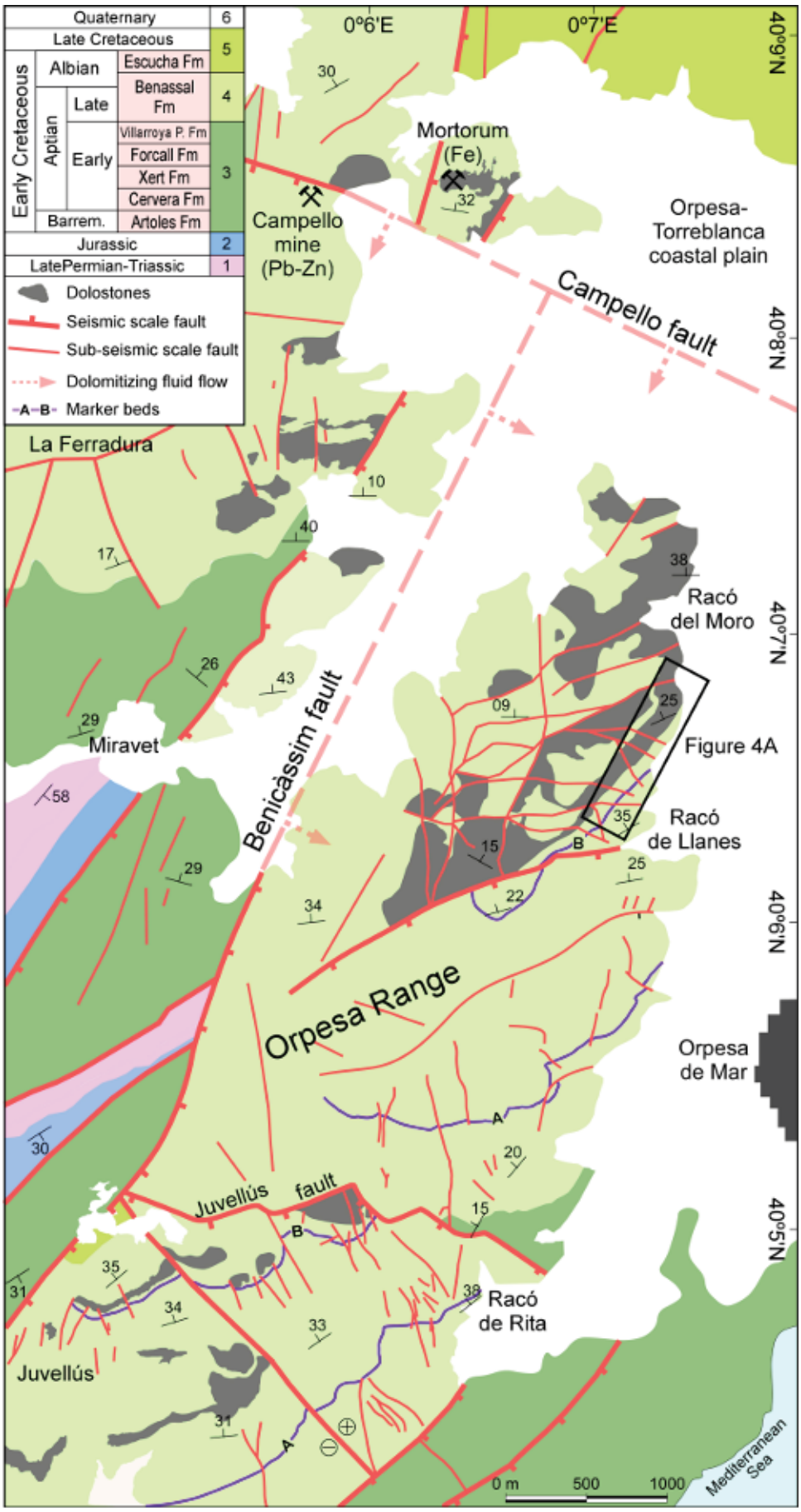


Figure 2: Geological map of the study area showing the distribution of dolostones in the Benassal Fm (modified from Martín-Martín et al. 2012a). Lithologies noted in the legend are: 1, red lutites and sandstones, dolostones, and gypsum; 2, dolomitic breccias, dolostones and limestones; 3, limestones and marls; 4, limestones, marls and dolostones; 5, quartz sandstones, clays, limestones, dolostones and marls; 6, conglomerates, sands and clays.

Dolomitization of the syn-rift succession exclusively affects the Late Aptian to earliest Albian Benassal Fm, which is a ∼1500-m-thick carbonate ramp succession formed almost entirely by shallow-water, marine deposits (Martín-Martín et al., 2010, 2013) (Figs. 2, 3 and 3). The succession is dominated by orbitolinid foraminifera, coral, and rudist bivalve fauna (Tomás, 2007; Tomás et al., 2007, 2008; Martín-Martín et al., 2013). The platform carbonates are stacked into three transgressive-regressive (T-R) sequences bounded by discontinuity surfaces of regional significance (Bover-Arnal et al., 2009). Rudist-rich lithofacies typically form the top of the T-R sequences, constituting excellent markers that can be followed throughout the study area (Martín-Martín et al., 2013) (Figs. 2 and 3). The top of the Benassal Fm is karstified and fossilized by the tidal clays and sands of the Escucha Fm, which has been interpreted to act as a regional seal for dolomitizing fluids (Martín-Martín et al., 2010).

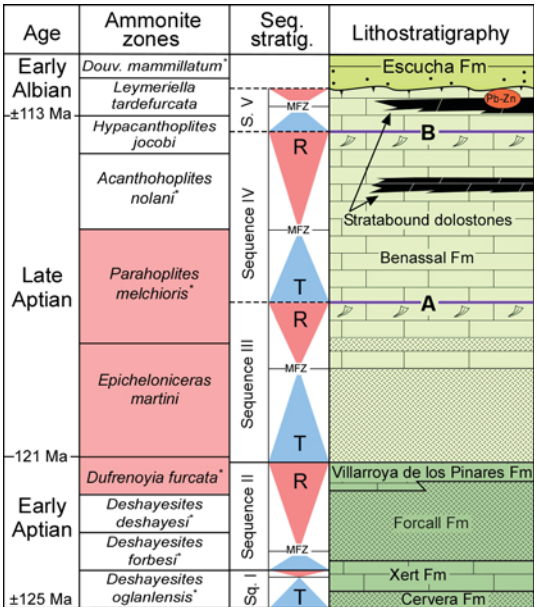


Figure 3: Chrono-, bio-, sequence- and lithostratigraphic chart of the Aptian succession of the Benicàssim area (modified from Martín-Martín et al., 2013). Ammonite biozones identified in the study area are shaded in red and those identified elsewhere in the Maestrat Basin with an asterisk (Martínez et al., 1994; Moreno-Bedmar et al., 2010; Garcia et al., 2014). Dashed lines in Transgressive-Regressive (T-R) sequences indicate lack of absolute dating and A-B violet lines denote marker beds (see figure 2 for location). MFZ, Maximum Flooding Zone; RST, Regressive System Tract; TST, Transgressive System Tract.

## 2.1 Dolostone distribution and geometry

Dolostones dominantly appear in hanging-wall blocks of both the NW-SE and NNE-SSW trending basement faults, forming two main seismic-scale, stratabound and tabular-shaped bodies with an individual maximum thickness of 150-m (Fig. 3 and 4A). These dolostone bodies can be recognized several kilometers away from the fault zones, extending for several thousand square meters over the study area (Fig. 2). Commonly, non-replaced mud-dominated limestones facies appear intercalated between the dolostone geobodies or bounding them (Fig. 4A-C). According Martín-Martín et al. (2013), these low-porosity facies facilitated the lateral fluid flow along higher porosity and more permeable units, enhancing the stratabound geometry of the dolostones away from the feeding faults. Dolomitization fronts are sharp and wavy and approximately follow the layer boundaries (Fig. 4B-C). However, the dolomitization fronts cross-cut the bedding planes, undulating up and down from centimeters to meters at the outcrop scale (Fig. 4E). These diagenetic

fronts frequently correspond to bedding-parallel stylolitic surfaces (Fig. 4F), indicating that stylolites acted as barriers for fluid flow during the replacement of the limestone. Less frequently, dolomitization fronts are constrained by meter-scale faults (source).

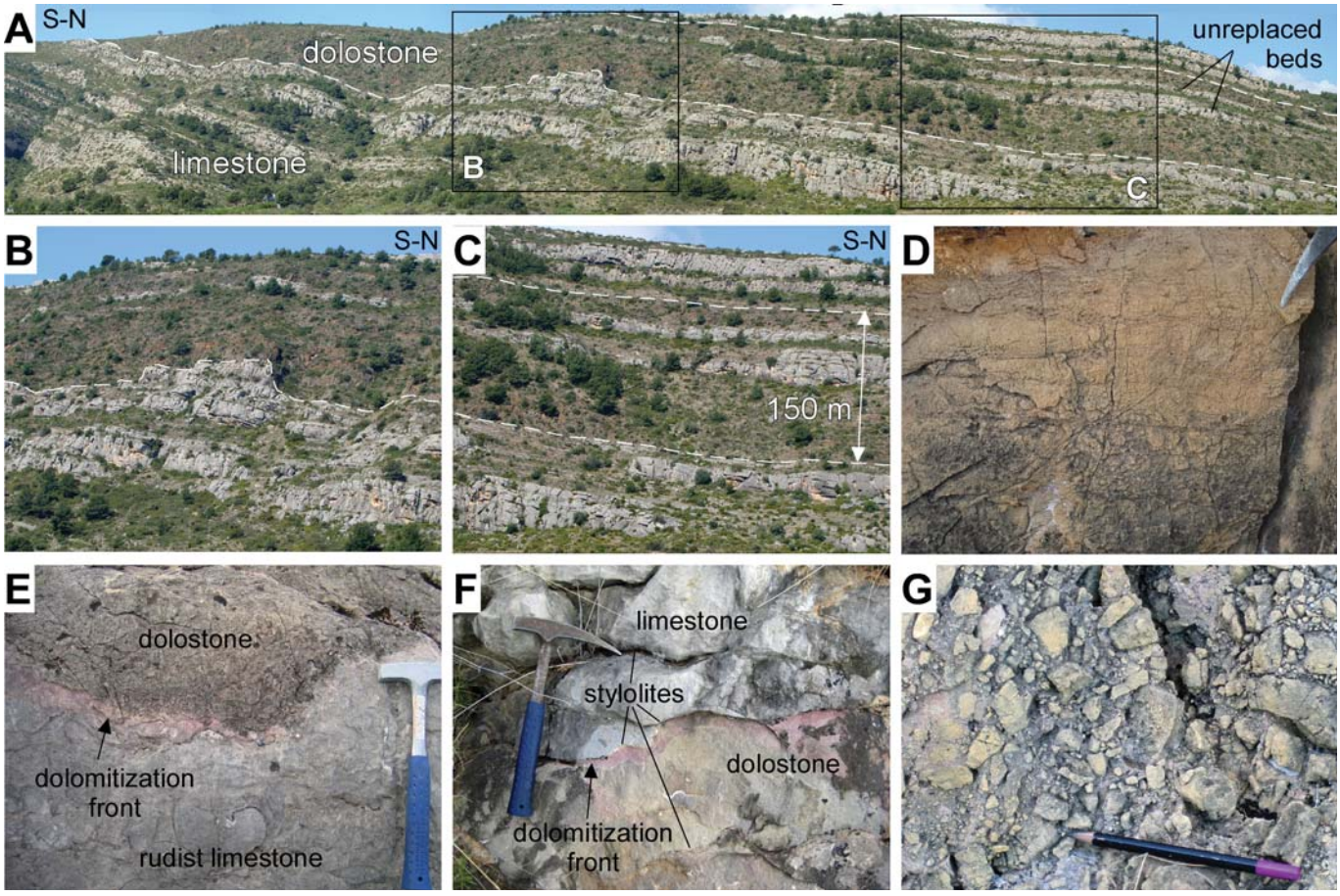


Figure 4: Field views of the Benassal Fm at Racó del Moro outcrop. (A-C) Spatial relationship between the host limestone (gray) and dolomites (brown). Note the stratabound dolomite bodies and the unreplaced limestone beds (stringers) between them; (D) Dolograinstone showing depositional lamination preserved after the replacement; (E) Typical sharp dolomitizing front between the host limestone and the dolostone; (F) Stylolite surfaces forming prominent dolomitizing fronts in muddy nodular facies. (G) Breccia made of dolostone clasts and cemented by late meteoric calcite cement in a sub-seismic scale fault zone.

## 2.2 Dolostone petrography and geochemistry

The Benassal Fm dolostones exhibit the typical burial paragenesis, which includes the replacement of the host limestones, cementation by burial dolomite and calcite, and MVT sulphide mineralization (Martín-Martín et al. 2010, 2013). The bulk of the dolostone is a replacive non-planar dolomite with a dominant fabric-retentive fabric. These dolostones have been interpreted to have originated from hydrothermal fluids based on the petrographic data and the oxygen isotopic composition of dolomite phases (Gomez-Rivas et al., 2010a; 2014; Martín-Martín et al. 2010, 2013; Corbella et al., 2014). Carbon-oxygen isotope model curves calculated in terms of fluid-rock interaction are consistent with formation of replacive dolomite between 80 and 110ºC, and precipitation of burial calcite at 80-120ºC (Gomez-Rivas et al., 2010a, 2014).

Mass balance calculations and geochemistry data applied to the Benicàssim case study suggest that seawater, either modified or pristine, and/or basement brines were the most

likely sources of magnesium for dolomitization (Gomez-Rivas et al., 2010a, 2014). Crush-leach data of fluid inclusion content in equivalent Aptian replacive dolomite from the Maestrat Basin supports the hypothesis that the dolomitizing fluid was most probably evolved seawater enriched with potassium during fluid circulation through the subsurface (Grandia, 2001; Grandia, et al. 2003). The emplacement of the MVT deposits in the Maestrat Basin is dated as Lower Paleocene (62.6±0.7 Ma; Grandia et al., 2000), constraining the timing of dolomitization of the Benassal Fm carbonates between the Early Albian (end of deposition) and the onset of the Tertiary. This time-span corresponds to the Late Cretaceous post-rift stage of the Maestrat Basin (Martín-Martín et al., 2010, 2012a, 2013). According to quantitative subsidence curves by Martín-Martín et al. (2010), burial depths of the affected rocks would have varied between 200 and 1000 m during that time. A post-rift dolomitization scenario is also postulated based on geochemical, reactive transport and fluid and heat flow numerical simulations applied to the Benicàssim case-study (Gomez-Rivas et al., 2010a, 2014; Corbella et al., 2014).

# 3 Methodology

202 samples were collected from outcrops along stratigraphic sections and perpendicular/parallel to faults planes. 185 samples were selected for thin section preparation and petrographic analysis by standard optical microscopy. Thin sections were half stained with alizarin red-S and potassium ferricyanide in order to facilitate the identification of ferroan and non-ferroan calcite, as well as dolomite phases. 40 thin sections were analyzed with cathodoluminescence microscopy with a Technosyn Cold Cathode Luminescence model 8200 MkII equipment, with operating conditions of 15-18 kV and gun current of 300-350 A. Dolomite types were recognized based on crystal size, crystal boundary shape (using the classification proposed by Sibley and Gregg (1987), inclusion content, cathodoluminescence color, and cross-cutting relationships. Textural characteristics of limestones and dolostones were investigated in detail with a scanning electron microscope (SEM) QUANTA 200 FEI equipped with a dispersive X-ray spectrometer (EDS).

Doubly-polished thin sections of selected samples were prepared and coated with carbon to allow analysis of major elements (Ca, Mg, Mn, Fe, Sr and Na) in a Cameca SX-50 electron microprobe equipped with four vertically distributed WDS spectrometers. Operating conditions were 20 kV of accelerating voltage, spot size of 10 m, and beam current of 6 nA (Ca, Mg, Si) and 40nA (Mn, Fe, Sr, Na). Detection limits were 495 ppm (Ca), 493 ppm (Mg), 131 ppm (Mn), 128 ppm (Fe), 161 ppm (Sr) and 128 (Na). Na and Mn data were under the detection limits for most diagenetic phases.

Oxygen and carbon stable isotopic composition was analyzed from 80 dolomite and calcite diagenetic phases. The isotopic signature of the host limestone was obtained by analyzing three samples of the micrite matrix and two samples of rudist shells that were little altered diagenetically (least-altered samples). Sampling was performed with a micro-drill equipped with 0.4 to 1 mm diameter bits. Powdered calcite and dolomite preparations were reacted with phosphoric acid for 3 and 15 min respectively in vacuum at 70 ℃. The evolved $CO_2$ was analyzed on a Thermo Finnigan MAT-252 mass spectrometer. Results were corrected and expressed in ‰ relative to standard Vienna Pee Dee Belemnite (V-PDB), reporting a precision of ± 0.02 ‰ for $\delta^{13}$C V-PDB and of ±0.04 ‰ for $\delta^{18}$O V-PDB.

$^{87}Sr/^{86}Sr$ isotopic ratio of 23 dolomite and calcite samples was analyzed, including replacive dolomite, saddle dolomite and dolomite cement, as well as calcite cement. Two samples of the least altered host rock micritic matrix and one rudist shell were analyzed in order to obtain the original host rock isotopic signature. Powders were converted to chlorides by leaching in acetic acid (10% in volume) and chlorhidric acid at several concentrations. The final liquid samples were loaded into chromatographic column with DOWEX 50Wx12 200/400 mesh cation exchange resin. A VG Sector 54 TIMS mass

spectrometer was used to analyze the isotopic composition of the isolated Sr. Results were controlled by repetitive analysis of the NBS-987 standard, averaging (n=11) 0.710202 ± 0.00004 (2), and normalized to $^{87}Sr/^{86}Sr = 0.1194$.

Melting ice and homogenization temperatures were measured in fluid inclusions using a Linkam THMS-600 heating-freezing stage. Due to the small size of the fluid inclusions, only those of calcite veins hosting sulfide mineralization (Campello mine; Fig. 2) were measured. For each inclusion, homogenization temperature always were measured prior to ice melting temperature. The equipment was calibrated with distilled water, 10 and 20% NACl solutions and pure $CO_2$ fluid inclusions, and the reproducibility of measurements below 0 ℃ was ±0.2 ℃ and ±2 ℃ for homogenization temperatures. Ice melting points were accurately determined following the sequential freezing method of Haynes (1985). Porosity and permeability measurements of representative limestones and dolostones were performed on cylindrical plugs of 20-mm (0.9 in) diameter and 57 mm (2.2 in) length drilled in rock samples both parallel and perpendicular to bedding. The total porosity was quantified by water porosimetry using the Archimedes method (see Cavailhes et al., 2013 for methodological details). The analytical accuracy is ±0.05%. Gas permeability was measured using a Hassler cell permeameter, steady-state flow method and nitrogen as fluid, under same conditions (confining pressure of 1.5 MPa and pore pressure of 1.4 MPa). The analytical accuracy varies between ±10% (k1 D) and ±0.5% (k0.001 mD).

# 4 Results

## 4.1 Petrography

### 4.1.1 Calcite cements 1 and 2 (CC1 and CC2)

Calcite cement CC1 occurs as very fine crystals ranging between 10 m and 80 m in size. CC1 forms isopachous rims that line primary interparticle porosity and fills intraparticle porosity in limestones (Fig. 5A). Calcite cement CC2 occurs as clear spar crystals between 50 m and 2 mm in size (Fig. 5A). CC2 fills primary interparticle, shelter, fenestral and burrow porosity in limestones, as well as secondary moldic porosity. In addition, CC2 forms frequent syntaxial overgrowths over echinoderm plates. CC2 engulfs concavo-convex grain contacts, and thus postdates the early stages of mechanical compaction.

### 4.1.2 Dolomite cement 1 (DC1)

Dolomite cement DC1 fills primary inter- and intraparticle porosity, and secondary moldic porosity in grain-dominated limestone facies (Fig. 5A-D). DC1 shows homogeneous light gray color under plane-polarized light, slightly undulose extinction, and bright to dull red luminescence. DC1 engulfs, and thus postdates, calcite cements CC1 and CC2, as well as mechanical compaction. DC1 dominantly occurs in peloidal and orbitolinid packstones to grainstones, and peloidal grainstones (see Martín-Martín et al., 2013 for facies description). Moreover, DC1 is also abundant in limestones in the proximity of the dolomitization front (up to 1-2 m from it), where it shows similar textural characteristics to the dolomite replacing matrix (Fig. 5C and D).

### 4.1.3 Replacive dolomite 1 (RD1)

Replacive dolomite RD1 occurs as transitional planar-s to non-planar-a crystals with cloudy appearance (inclusion rich) and polymodal size distribution (Fig. 6A). Most replacive mass is fine to coarsely crystalline in size (50-600 m) although considerably larger crystals (500-3000 m) are also observed. These larger dolomite crystals resulted from the replacement of large-size echinoderm plates (Fig. 6B-C). RD1 crystals show light

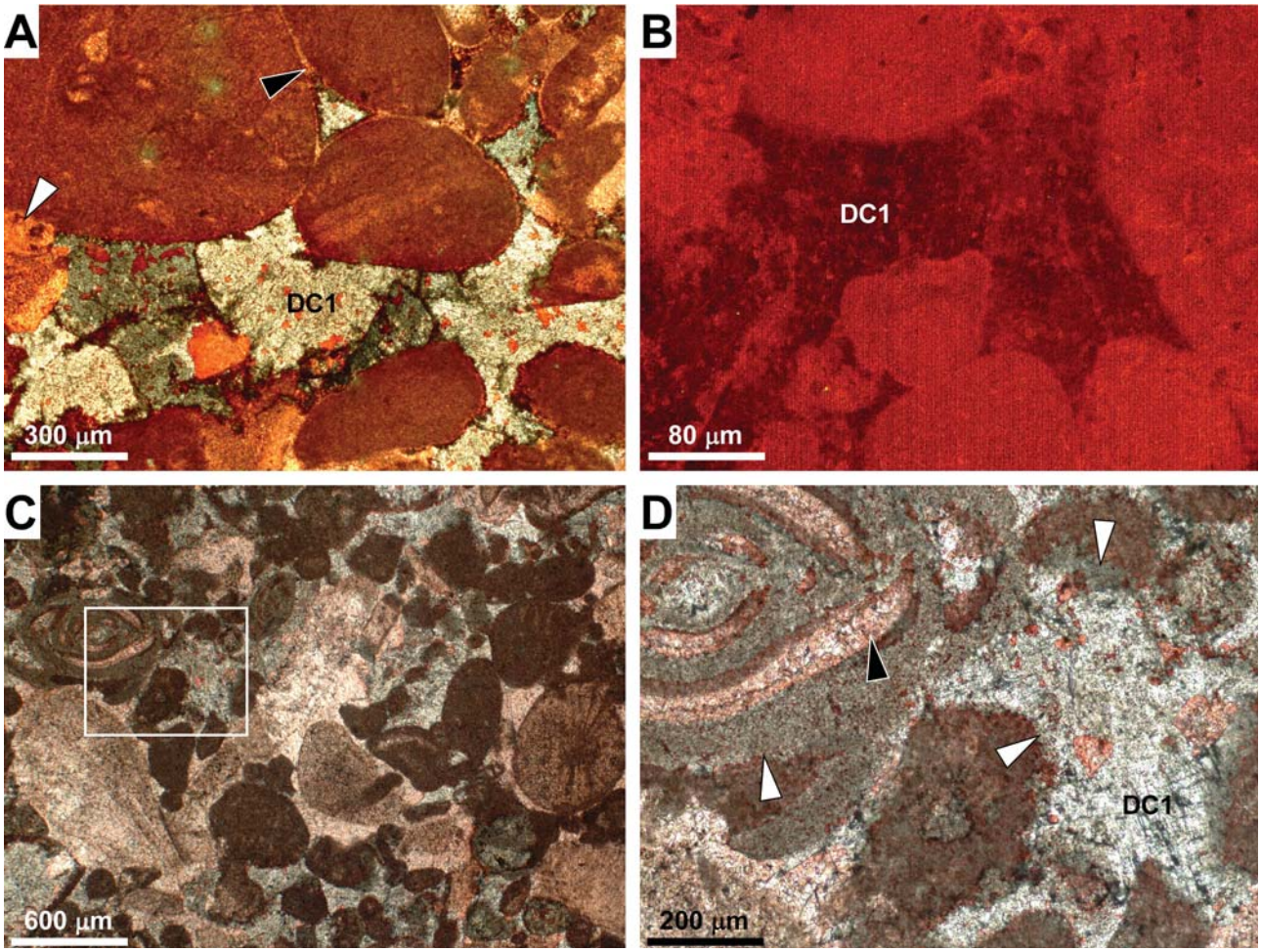


Figure 5: Photomicrographs of dolomite cement DC1 showing: (A) DC1 filling primary interparticle porosity in a peloidal grainstone, and postdating calcite cement CC1 (black arrow) and CC2 (white arrow). Stained with Alizarin red S. Plain light; (B) Typical dull red luminescence color; (C) DC1 filling primary interparticle porosity in a peloidal and bioclastic packstone. Stained with Alizarin red S. Plain light; (D) Close view of C denoting that peloids and miliolids are partially replaced (white arrows) whereas calcite cement appear unreplaced (black arrow). Plain light.

gray color under plane-polarized light, undulose extinction, and speckled dull red luminescence (Fig. 6D). Staining with K-ferricyanide indicates that RD1 crystals are ferroan to slightly ferroan. RD1 postdates stylolitization. RD1 forms tight crystal mosaics that exhibit scatter sub-millimetric intercrystalline porosity (mesopore to micropore according to Choquette and Pray, 1970). Individual RD1 crystals show abundant intracrystalline porosity (micropores following Choquette and Pray, 1970) and remnants of the host limestones (Fig. 6E-F).

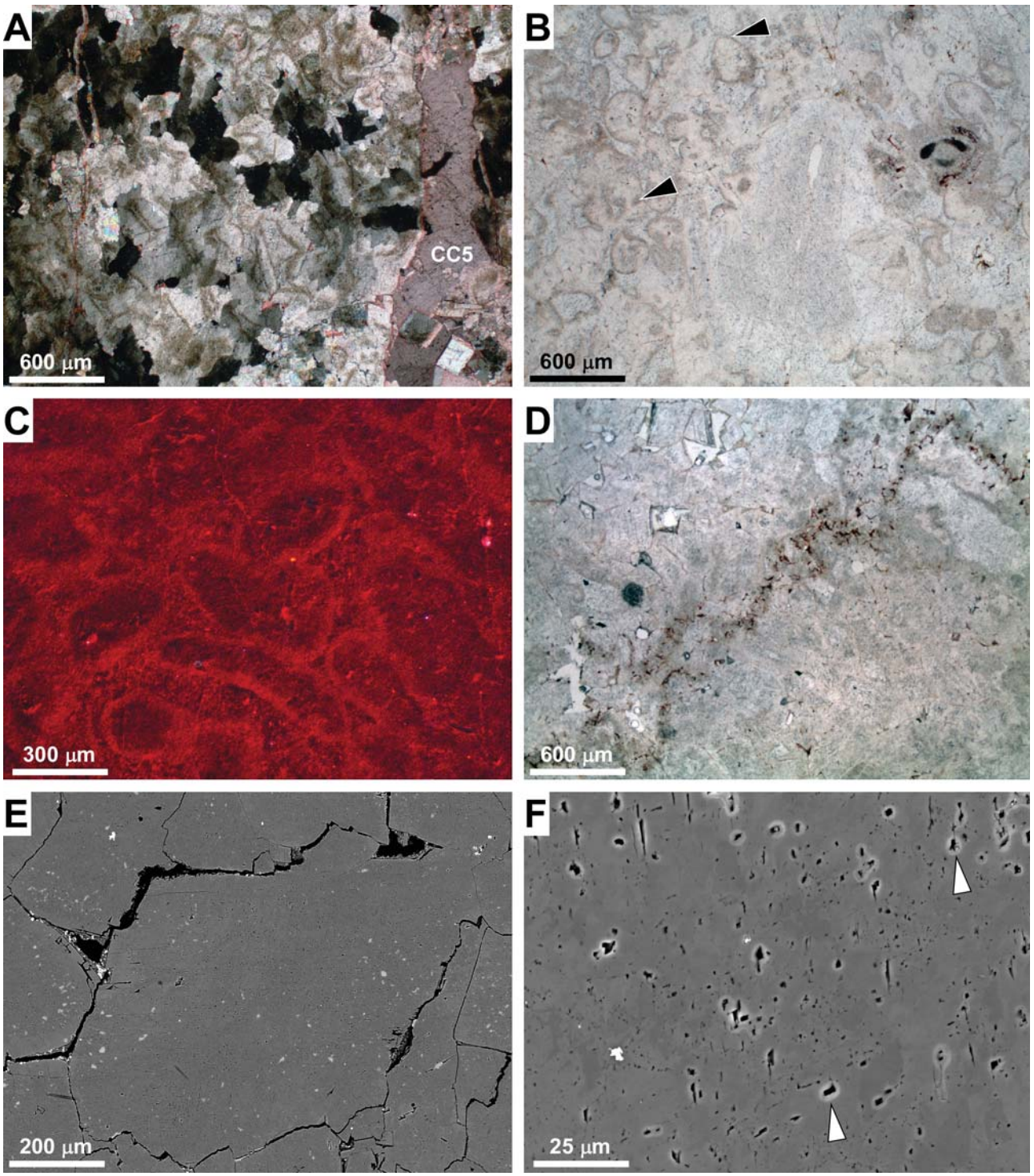


Figure 6: Photomicrographs of replacive dolomite RD1 showing: (A) Planar-s to non-planar-a crystal mosaic. Crossed nicols; (B) Fabric-retentive texture denoting the replacement of a peloidal grainstone. Note the concavo-convex contact between components evidencing compaction before replacement (black arrows). Diffused light; (C) Characteristic dull to bright red luminescence color of RD1 crystals; (D) Replacive dolomite crystal mosaic showing the smoothed trace (brown) of a stylolite. The brown color corresponds to the remains of the insoluble residue engulfed by RD1 crystals. Diffused light; (E) RD1 dolomite crystals with high intracrystalline microporosity and remnants of the host limestone; (F) Detail of the abundant microporosity typical of RD1 crystals (white arrows). Note the variation in Ca/Mg of the dolomite crystal by grey colors.

RD1 pervasively replaces matrix, grains and early calcite cements in both mud- and grain-dominated facies. The replacement of the host limestone is mostly mimetic, being skeletal and non-skeletal components clearly recognized in thin section (Fig. 6B-C). Mimetic textures evidence the preferential replacement of bioclastic wackestones-packstones, peloidal grainstones, and orbitolinid mudstones-rudstones. The replacement of grain-dominated facies is also evidenced by the presence of green grains (i.e. glaucony) within RD1 crystal mosaics. Additionally, RD1 partially replaces matrix, skeletal and non-skeletal components in limestones up to 20-30 cm away from the dolomitization front.

### 4.1.4 Replacive dolomite 2 (RD2)

Replacive dolomite RD2 occurs in completely dolomitized facies forming medium to coarse (100 m to 1.6 mm) planar-s to non-planar-a crystal mosaics (Fig. 7A and B). RD2 crystals are frequently formed by a RD1 cloudy core and a clear crystal outer part. Relics of skeletal and non-skeletal components are distinguished within these cores (Fig. 7A). Patches of the primary RD1 crystal mosaics often occur within mosaics of RD2, suggesting a textural evolution from one to the other (Fig. 7A and D). RD2 is considerably less abundant than RD1, and appears closely associated with fractures and other highly permeable areas.

RD2 crystals are gray in color under plane-polarized light and exhibit an overall homogenous dull to bright red luminescence (Fig. 7C). RD2 displays straight extinction although it can be slightly undulose when RD1 crystal cores are present. RD2 mosaics show abundant intercrystalline porosity along crystal margins and intersections (Fig. 7D and E). Pore size range from micropores to mesopores sensu Choquette and Pray (1970). The RD2 clear outer part has less intracrystalline microporosity and fewer solid inclusions than the cloudy core of RD1 (Fig. 7E and F).

### 4.1.5 Dolomite cement 2 (DC2)

Dolomite cement DC2 appears in the form of clear syntaxial overgrowths on cloudy RD1 and RD2 crystal centers, and lining RD1/RD2 mosaics, fractures and molds in dolostones (Fig. 8A-D). It resulted in planar-e crystal mosaics with individual crystals ranging from fine to very coarse in size (100-1500 m) (Fig. 8B). DC2 commonly form a thin rim, although occasionally up to four rim overgrowths can be distinguished. DC2 is light gray in color under plane-polarized light and shows a bright orange to red luminescence (Fig. 8C-D). Compared to replacive dolomites, DC2 has notably fewer solid inclusions and lower intracrystalline microporosity (Fig. 8E and F).

### 4.1.6 Saddle dolomite 1 (SD1)

Saddle dolomite SD1 occurs as coarse to very coarse (400-5000 m) non-planar crystals with typical curved boundaries and undulose extinction (Fig. 9A). SD1 crystals show gray color under plane-polarized light and dull red luminescence (Fig. 9B). Staining with K-ferricyanide indicates that SD1 crystals are slightly ferroan. SD1 overgrowths RD1 crystals (Fig. 9A), and appears as pore-lining in fracture and solution enlarged stylolitic and vuggy porosity in dolostones (Fig. 9C-E). Moreover, it occurs as pore-filling in fracture, shelter, and moldic porosity in limestones. SD1 is more abundant in limestones located next to faults and/or dolomite bodies. SD1 is recognized by its white color in hand specimen that changes to pinky or brown when partially or completely calcitized, respectively.

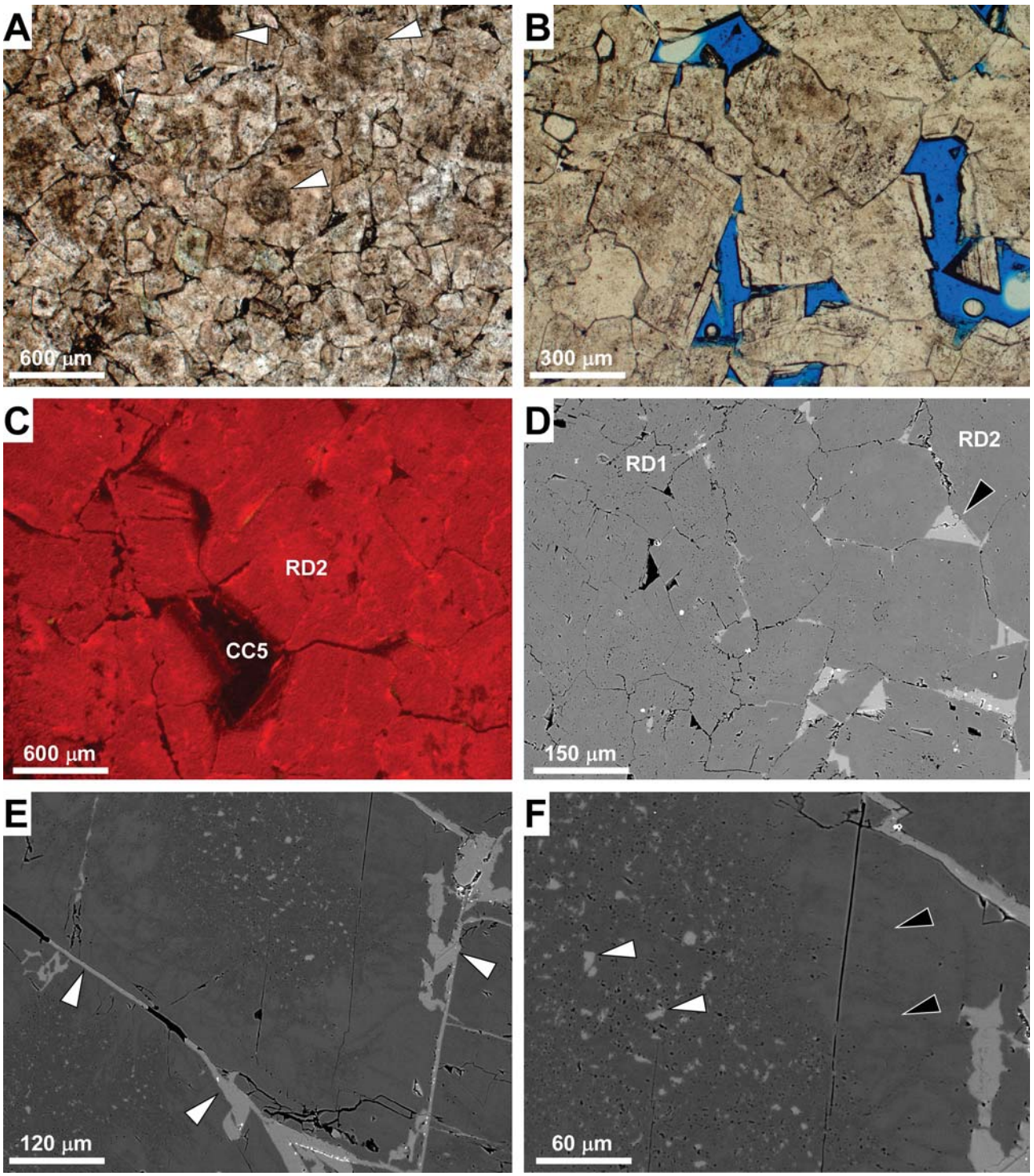


Figure 7: Figure 7. Photomicrographs of replacive dolomite RD2 showing: (A) Planar-s to non-planar-a RD2 crystal mosaic with cloudy RD1 relics (white arrows). Plain light; (B) RD2 crystal mosaic showing intercrystalline porosity at crystal junctions. Plain light; (C) Homogenous bright red luminescence color. (D) Transition between RD1 and RD2 crystal mosaics. Note the evolution from interboundary pores in RD1 to tetrahedral pores (arrowed) in RD2 (pore classification following Wardlaw, 1976); (E) RD2 dolomite crystal with porosity along crystal edges and junctions partially filled with calcite cement CC5 (white arrows); (F) Detail of the dolomite crystal in E (upper right corner) showing the transition between the microporous core (white arrows) and the less porous border (black arrows). Note the remnants of the host limestone within the Rd1 core.

### 4.1.7 Calcite cement 3 (CC3)

Calcite cement CC3 occurs as clear euhedral to subhedral blocky crystals ranging between 100 m and 7 mm in size (Fig. 9C-E). CC3 has a bright orange to yellow zoned luminescence (Fig. 9F). CC3 fills intercrystalline porosity in dolostones, and solution enlarged vugs, stylolitic and fracture porosity in dolostones and limestones (Fig. 9C-E). CC3 engulfs, and thus postdates, replacive dolomites (RD1 and RD2) and dolomite cements (DC2 and SD1) (Fig. 9D).

### 4.1.8 Calcite cement 4 (CC4)

Calcite cement CC4 occurs as clear euhedral to subhedral crystals, ranging between 100 and 1500 m in size. CC4 has bright to dull yellow zoned luminescence. CC4 fills vertical fractures and the remaining vuggy porosity after SD1 and CC3 cementation.

### 4.1.9 Calcite cement 5 (CC5)

Calcite cement CC5 occurs as subhedral to anhedral crystals ranging between 100 and 2500 m in size, and is non-luminescent (Fig. 8A). CC5 pervasively fills vuggy and intercrystalline porosity in dolostones, replaces dolomites, and fills fracture porosity in both limestones and dolostones (Fig. 10A and B). Moreover, CC5 extensively cements dolomitic breccias in subseismic-scale fault zones along dolostone geobodies (Fig. 4G). CC5 engulfs, and thus postdate all dolomites phases and calcite cements.

Calcitization (dedolomitization) affects all dolomite types and is more extensive at outcrop surfaces, in the vicinity of faults, and along open fractures and stylolites. The CC5 selectively replaces the inner rim overgrowth and/or the cloudy core of rhombohedral DC2 crystals (Fig. 10B). Partial calcitization is distinguished by bright luminescent calcite zones within dolomite crystals. Completely calcitized dolomite areas are recognized in outcrop by their brown to orange color. At micro-scale thin coatings of Fe-oxide appear on the edges of remaining dolomite crystals and filling the porosity.

### 4.1.10 Calcite cement 6 (CC6)

Calcite cement CC6, actually a succession of calcite and dolomite bands, occurs as concentric crystal aggregates with a dominant pendant texture (Fig. 10C-D). CC6 fills millimeter-sized vugs, and dissolution enlarged fracture and stylolitic porosity within dolomite and calcitized dolomite crystal mosaics. Dolomite bands typically show a fibrous radial structure.

### 4.1.11 Other diagenetic phases

Together with the calcite and dolomite diagenetic phases reported above, silica-bearing minerals and MVT sulphide minerals are also present in the Benassal Fm. Opal-CT and quartz are common throughout the succession typically replacing skeletal components such as corals in coral-bearing facies. Silicification is only observed in limestones, and thus mainly pre-dates the replacement stage. MVT deposits hosted in the Benassal Fm contain the following mineral paragenesis: galena, sphalerite, barite, goethite, hematite, pyrite, calcite and dolomite. These minerals fill fractures and voids in dolostones, or they fill secondary porosity in karstic sediments constituted by sand sized limestone and quartz, and mica clasts.

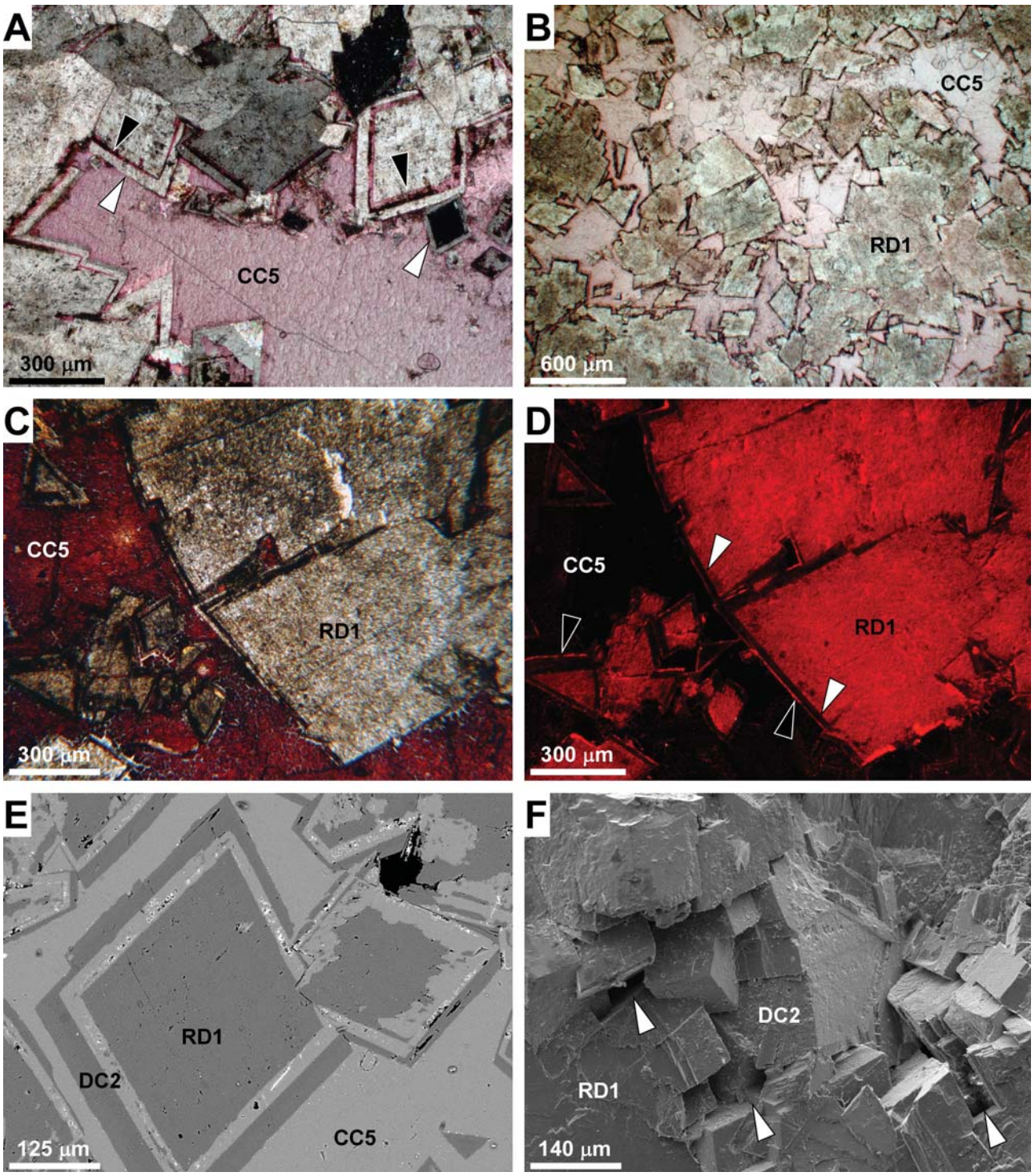


Figure 8: Photomicrographs of dolomite cement DC2 showing: (A) DC2 rim overgrowths (white arrows) lining replacive dolomites and forming planar-e crystals. Note that the inner rim overgrowth (black arrows) is selectively replaced by calcite CC5. Stained with Alizarin red S. Crossed nicols; (B) DC2 overgrowths lining (brown color) dolomite RD1 crystal mosaics. Note that the original intercrystalline porosity is completely filled by late calcite cement CC5. Crossed nicols; (C-D) Photomicrographs and CL pair showing the characteristic bright to dull red color of DC2 (black arrows). Note the non-luminescent character of the calcitized dolomite (CC5) inner overgrowth (white arrows); (E) DC2 crystal mosaic with intercrystalline porosity destroyed by calcite cement CC5. Note that CC5 selectively replaced the inner rim overgrowths; (F) Tetrahedral pores system typical of the DC2 crystal mosaic (white arrows).

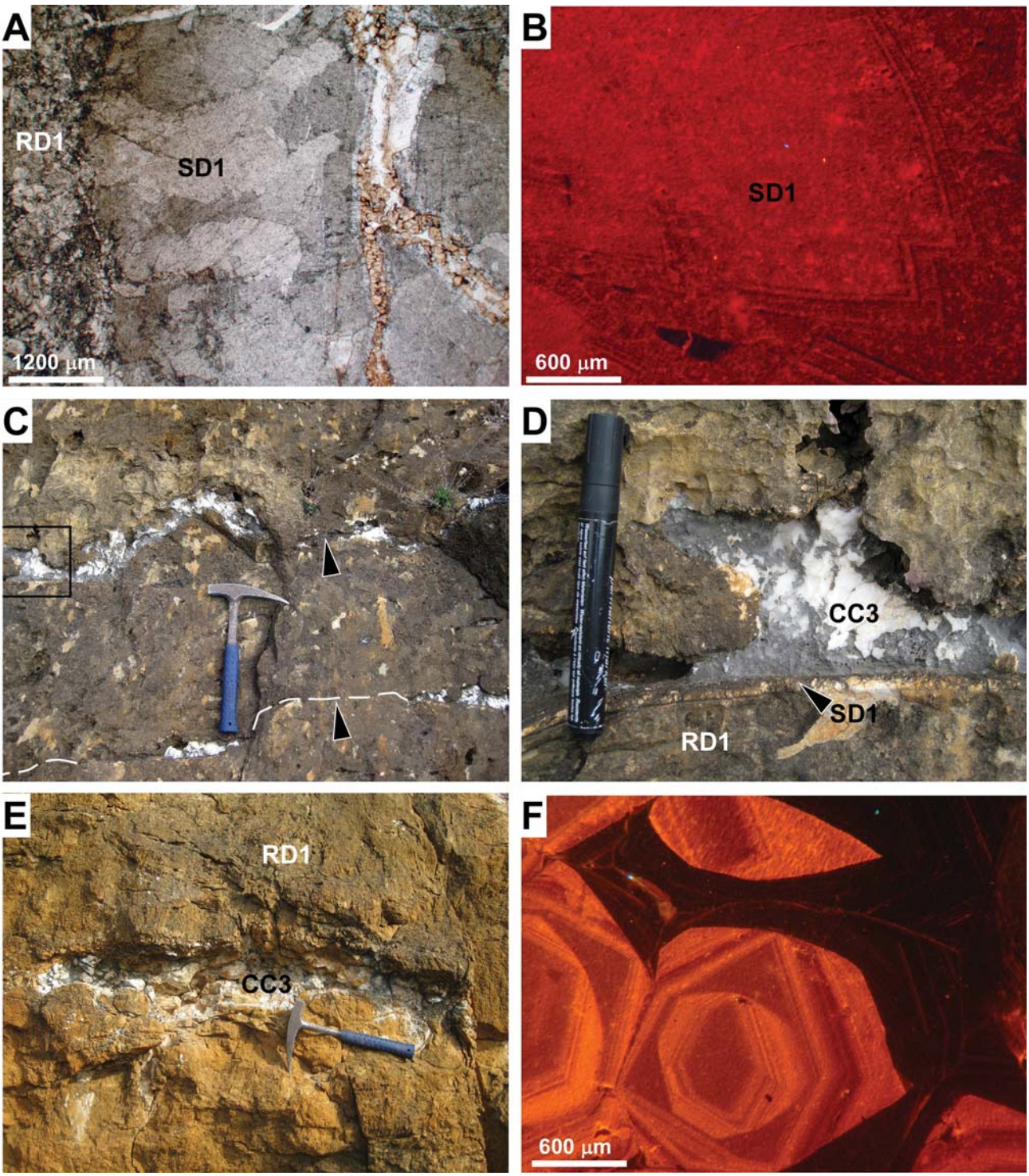


Figure 9: Photomicrographs and field images of saddle dolomite cement SD1 and burial calcite cement CC3 showing: (A) SD1 filling a fracture in a RD1 crystal mosaic. Plain light; (B) Dull red luminescence color, with thin zonation, typical of SD1; (C) Parallel to bedding set of solution enlarged stylolites (black arrows) filled with CC3 (white); (D) Close up of image C (black rectangle) showing SD1 rimming and CC3 infilling the solution enlarged stylolite; (E) CC3 completely filling a meter-scale mesovug in a replacive dolostone; (F) Orange to brown concentric CL zonation of CC3 crystals.

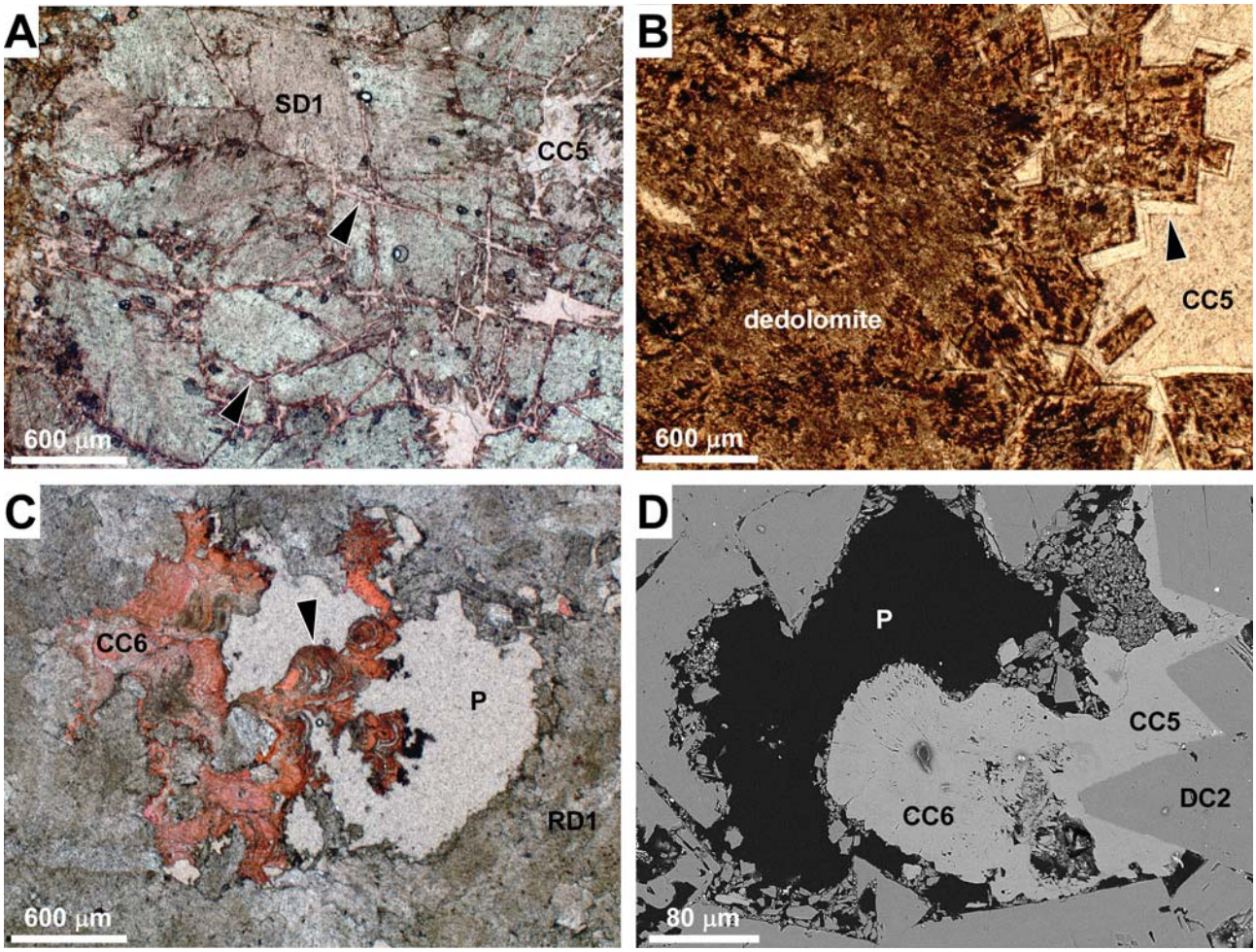


Figure 10: Photomicrographs of calcite cement CC5 and CC6 showing: (A) SD1 crystals slightly calcitized along cleavage planes (black arrow). Thin section stained with Alizarin red S. Plain light; (B) Replacive dolomite crystal mosaic strongly calcitized (CC5). Note that only DC2 rim overgrowths remain unaltered (black arrow). Plain light; (C) CC6 partially filling vuggy porosity (P). Note the calcite and dolomite bands after staining with Alizarin red S. Plain light; (D) BSE image of CC6 postdating dissolution of CC5 and rhombohedral DC2 crystals.

## 4.2 Geochemistry

### 4.2.1 Major elements

All reported dolomites in the Benicàssim area are nonstoichiometric, calcium-rich and have variable but relatively high Fe content (Table 1). The Fe concentration is commonly higher in replacive dolomites (RD1 and RD2) and dolomite rim overgrowths (DC2) than in saddle dolomite SD1.

CC2 exhibits Sr content up to 600 ppm, and low concentration of Mn, Fe and Na (Table 2). CC3 contains variable but relatively high contents of Fe, Mn and Sr, whereas CC4 show variable but relatively high Sr, moderate Fe, and low Mn and Na contents. CC5 shows variable but relatively high Sr, Fe and Na, and low Mn concentration. CC6 chemistry is not available but those dolomite bands intercalated in between (Fig. 10C) are characterized by low Fe, Mn, and Sr contents, and high Na content (Table 2).

| | | CaCO3 (wt%) | MgCO3 (wt%) | Fe (ppm) | Mn (ppm) | Na (ppm) | Sr (ppm) |
|---|---|---|---|---|---|---|---|
| | Max. | 76.0 | 44.7 | 9.528 | 230 | 2213 | 1.319 |
| DC1 | Min. | 54.7 | 21.6 | 800 | bdl | bdl | 200 |
| | Mean | 60.1 | 38.7 | 4290 | 122 | 370 | 681 |
| | Max. | 60.4 | 44.4 | 28.600 | 800 | 722 | 944 |
| RD1 | Min. | 50.4 | 38.2 | 1.744 | bdl | bdl | bdl |
| | Mean | 55.5 | 42.6 | 8.016 | 328 | 150 | 478 |
| | Max. | 58.7 | 45.4 | 21.498 | 849 | 1.200 | 1.040 |
| RD2 | Min. | 53.3 | 38.8 | 2.400 | 100 | bdl | bdl |
| | Mean | 55.1 | 42.7 | 9.105 | 394 | 127 | 399 |
| | Max. | 58.0 | 44.3 | 21.575 | 871 | 200 | 1.039 |
| DC2 | Min. | 53.1 | 40.7 | bdl | bdl | bdl | 200 |
| | Mean | 55.6 | 42.3 | 10.728 | 374 | 36 | 694 |
| | Max. | 62.5 | 45.4 | 12.273 | 370 | 1.004 | 1.242 |
| SD1 | Min. | 53.5 | 36.7 | 1.805 | bdl | bdl | bdl |
| | Mean | 58.1 | 41.0 | 4.416 | 112 | 207 | 757 |

Table 1: Elemental composition (microprobe data) of the investigated dolomite phases.

| | | Ca (ppm) | Mg (ppm) | Fe (ppm) | Mn (ppm) | Na (ppm) | Sr (ppm) |
|---|---|---|---|---|---|---|---|
| | Max. | 40.7200 | 2.655 | bdl | 200 | 200 | 615 |
| CC2 | Min. | 39.6381 | 700 | bdl | bdl | bdl | bdl |
| | Mean | 40.2893 | 2.032 | bdl | 104 | 119 | 418 |
| | Max. | 41.1603 | 4.597 | 4.393 | 684 | 165 | 2.579 |
| CC3 | Min. | 39.0222 | bdl | bdl | bdl | bdl | 1.194 |
| | Mean | 40.3836 | 1.937 | 744 | 108 | 65 | 1.575 |
| | Max. | 40.7011 | 5.374 | 653 | 243 | 295 | 1.767 |
| CC4 | Min. | 39.1084 | 460 | bdl | bdl | bdl | 447 |
| | Mean | 39.9516 | 2.139 | 225 | 88 | 56 | 845 |
| | Max. | 41.1930 | 5.700 | 2.200 | 299 | 556 | 1.766 |
| CC5 | Min. | 38.2400 | bdl | bdl | bdl | bdl | bdl |
| | Mean | 39.9203 | 2.784 | 321 | 50 | 85 | 773 |
| | Max. | 27.5900 | 144.100 | 189 | 664 | 500 | 291 |
| CC6 | Min. | 19.3800 | 87.400 | bdl | bdl | bdl | bdl |
| | Mean | 23.1445 | 116.991 | 56 | 168 | 164 | 138 |

Table 2: Elemental composition (microprobe data) of the investigated calcite phases. Note that CC6 data only correspond to dolomite-rich bands.

### 4.2.2 Stable isotopes

The least altered rudist shells (n=2) yielded $\delta^{18}$O V-PDB values between -3.77 and -2.53‰ and $\delta^{13}$C V-PDB values between +5.44 and +6.23‰, while the micritic matrix (n=3) give $\delta^{18}$O V-PDB values between -5.50 and -2.72‰ and $\delta^{13}$C V-PDB values between +4.08 and +4.39‰ (Fig. 11). In both cases the resulting analytical range is close to the original isotopic composition of the Lower Cretaceous marine carbonates (Allan and Wiggins, 1993).

Cement and replacive dolomites yielded $\delta^{18}$O V-PDB values between -6.18 and -10.51‰, and $\delta^{13}$C V-PDB values between +1.89 and +5.75‰ (Fig. 11). Progressively depleted values of $\delta^{18}$O are recorded from dolomite cement DC1 (mean -6.92‰; n=9)

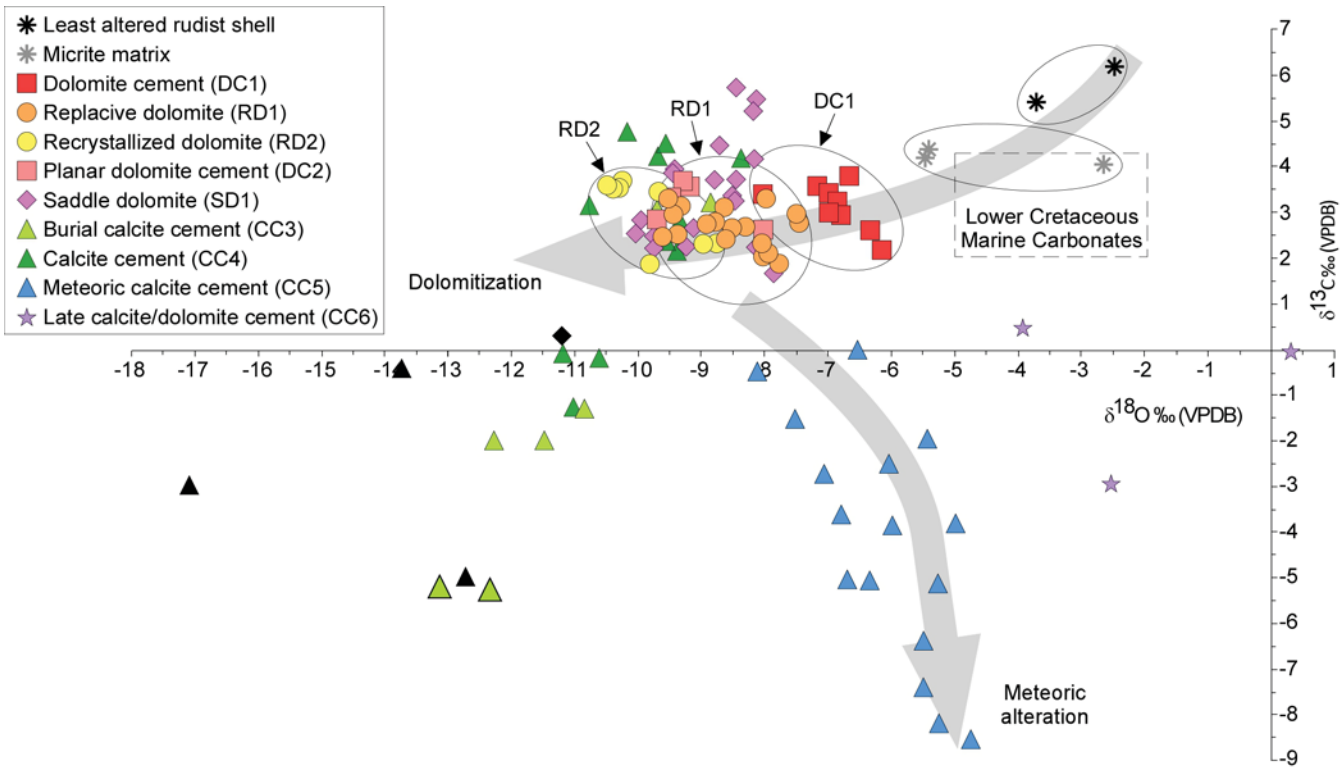


Figure 11: $\delta^{18}$O vs $\delta^{13}$C plot of Aptian host limestones and diagenetic dolomite and calcite phases. Black triangles and diamonds correspond to saddle dolomite SD1 and calcite cement CC3from the MVT site after Gomez-Rivas et al. (2014). Lower Cretaceous marine carbonates signature according to Allan and Wiggins (1993).

to replacive dolomite RD1 (mean -8.55‰; n=19), and to replacive dolomite RD2 (mean -9.86‰; n=8). Saddle dolomite SD1 give intermediate $\delta^{18}$O V-PDB values between replacive dolomites RD1 and RD2 (mean -8.76‰; n=17). Dolomite cement DC2 shows intermediate values as well (mean -9.17‰; n=5), partially due to contamination with the dolomite crystal core during sampling. Most calcite cement CC3 yielded $\delta^{18}$O V-PDB values (-9.72 to -8.71‰) and $\delta^{13}$C V-PDB values from +3.06 to +3.60‰ similar to those reported above for dolomites (Fig. 11). Highly depleted $\delta^{13}$C V-PDB values of CC3 (from -2.03 to -1.31‰) and $\delta^{18}$O V-PDB values (from -12.36 to -10.87‰) are recorded from calcite cements filling megapores and fractures close to major faults. Calcite cement CC4 $\delta^{18}$O V-PDB signature varied from -10.78 to -8.39‰ and $\delta^{13}$C V-PDB from -1.36 to +4.60‰. Calcite cement CC5 yielded $\delta^{18}$O V-PDB values between -8.09 and -4.78‰, and $\delta^{13}$C V-PDB values between -8.59 and +0.09‰ (Fig. 11). Significantly higher $\delta^{18}$O V-PDB (-3.96 to +0.29‰) and $\delta^{13}$C V-PDB (-2.99 to +0.04‰) values are registered in calcite CC6 compared to other reported cements.

### 4.2.3 Strontium isotopes

The $^{87}$Sr/$^{86}$Sr ratio of the micritic matrix and rudist shell ranges between 0.70720 and 0.70732, which is in agreement with the range reported in the literature for the Aptian-Albian seawater (Jones and Jenkyns, 2001) (Fig. 12). Replacive dolomite RD1 Sr ratios range from 0.70748 to 0.70762 (n=7), while replacive dolomite RD2 show a relatively constant value around 0.70766 (n=2) corresponding to the upper limit of the RD1 range. Saddle dolomite SD1 Sr isotopic composition is between 0.70746 and 0.70753 (n=2).

Calcite cement CC3 $^{87}$Sr/$^{86}$Sr data range from 0.70756 to 0.70761 (n=2), and that of calcite cement CC4 is around 0.70734 (n=1) (Fig. 12). Calcite cement CC5 Sr ratios range between 0.70765 and 0.70790 (n=4).

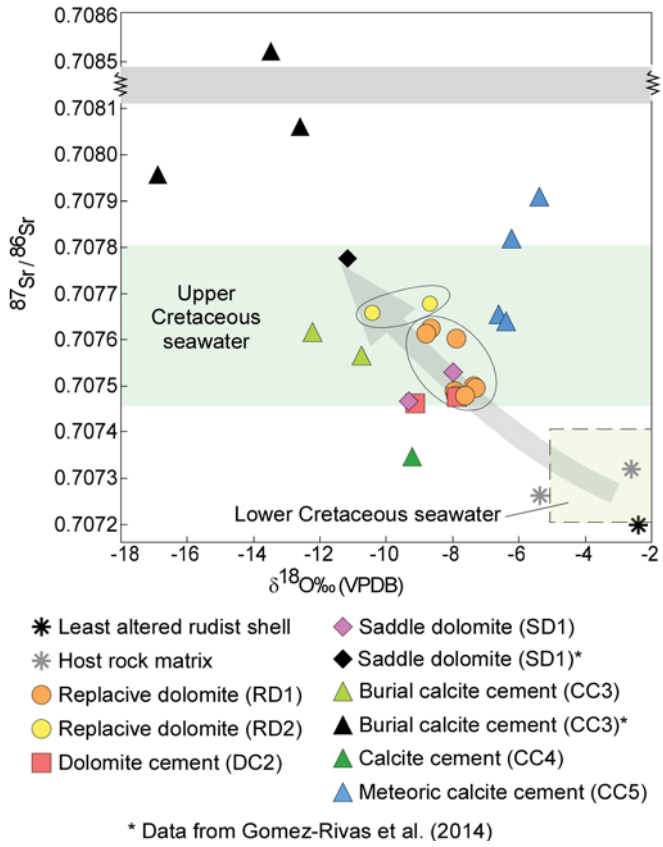


Figure 12: $^{87}Sr/^{86}Sr$ vs $\delta^{18}O$ plot showing the increase in radiogenic strontium of RD1, SD1, RD2 and CC3 compared with the host rock and least altered rudist shells. The trend is noted with an arrow. Aptian-Albian and Upper Cretaceous seawater signature according to Jones and Jenkyns (2001). Note that the Late Cretaceous signature does not represent any specific oxygen isotope value.

## 4.3 Fluid inclusion microthermometry

Primary fluid inclusions in CC3 (ore-stage calcite after Gomez-Rivas et al., 2014) range in size between 10 and 20 m. Ice melting temperatures (Tmi) range between -17.8 and -23.5 ℃ (n=14), which implies a salinity of 20.8 to 24.6 wt % NaCl eq. according to the NaCl-$H_2O$ calculation method of Bakker (2003) (Fig. 13). Due to the small size of these inclusions it was not possible to measure the melting temperature of hydrohalite ($NaCl{\cdot}2H_2O$). Homogenization temperatures (Th) are variable and range between 134 and 189.5 ℃.

## 4.4 Porosimetry and permeability

Unreplaced limestones have low porosity (<5%) and permeability (<1 mD) regardless of the facies (mud- vs grain-dominated) or sampling direction (parallel vs perpendicular to bedding) (Fig. 14). Significant higher porosity values appear in cross-bedded peloidal and orbitolinid packstones to grainstones (up to 6.7%) compared to other reported facies. Permeability values up to 0.9 mD appear in limestone samples measured perpendicular to bedding due to the presence of small vertical cracks that do not cause a significant porosity increase but notably affect permeability.

Dolostones show an overall increase in porosity and permeability compared to the host limestone (Fig. 14). Distribution of porosity and permeability in dolostones shows that any increase in porosity is associated with an increase in permeability, thus suggesting that these rocks have a better-connected pore system (i.e. intercrystalline porosity) than limestones. Permeability values of dolostones are generally higher along the direction perpendicular to bedding, which is related to the presence of small-scale fractures. Poros-

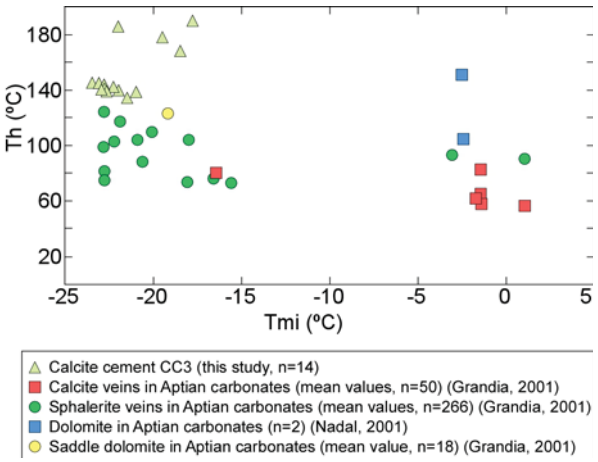


Figure 13: Homogenization vs ice melting temperatures of fluid inclusions measured from ore-stage calcite veins in Benicàssim (this study) compared to other authors data from the Maestrat basin (calcite and dolomite).

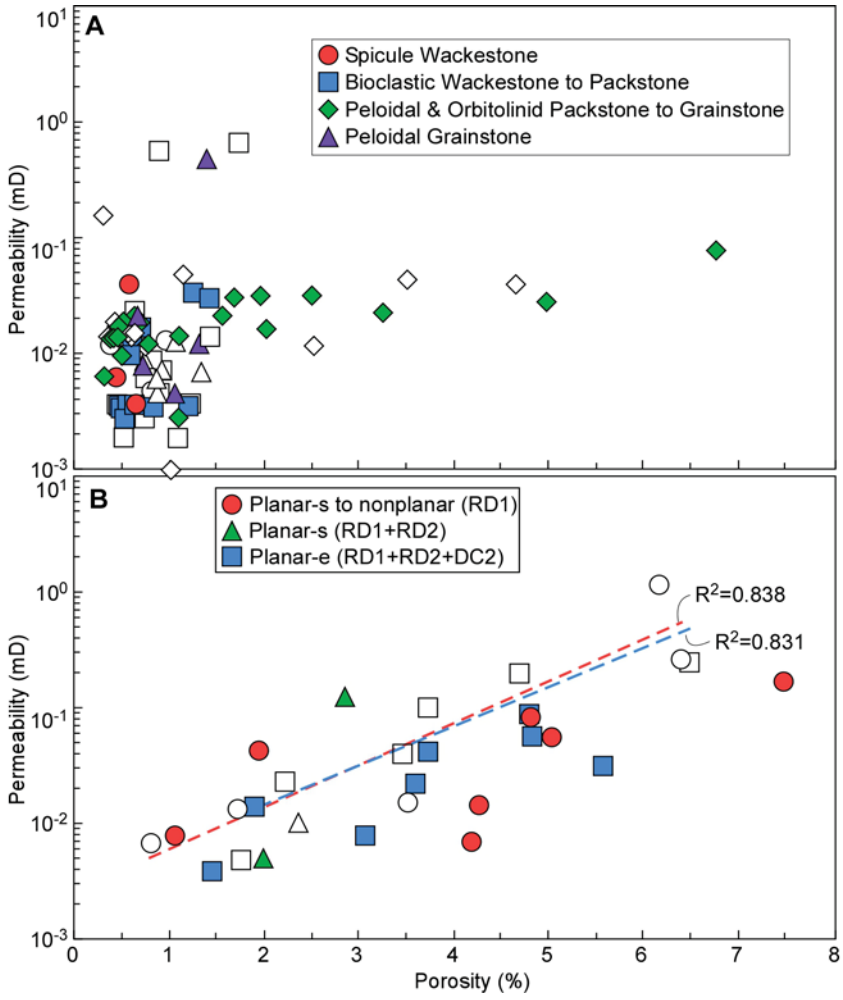


Figure 14: Porosity vs Log-permeability plot of selected limestone and dolostone samples based on (A) carbonate facies and texture, and (B) dolomite crystal texture. Closed and open symbols represent parallel and perpendicular to bedding data, respectively. Note the relatively strong correlation between porosity and permeability in the planar-s to nonplanar (red dashed line) and planar-e (blue dashed line) texture samples measured perpendicular to bedding.

ity/permeability distribution based on dolomite crystal texture shows higher values in samples characterized by a replacive dolomite 1 texture, which register a maximum value

of 7.4% and 1.6 mD.

# 5 Discussion

## 5.1 Paragenetic sequence

Field and analytical data indicate that the diagenetic evolution of the Benassal Fm limestones involve alterations occurring at shallow burial (early calcite cementation), intermediate to deep burial (dolomitization of the host limestones, and carbonate cementation associated with the emplacement of the MVT) and during uplift (late calcite cementation) (Fig. 15). The early cementation by calcite, which is the most important alteration that took place before the replacement stage, occurred shortly after deposition in a marine environment. In particular, the early near-surface marine diagenetic products include micrite envelops and isopachous fringe cement (CC1), both predating mechanical compaction (Fig. 5 and 15). In addition, calcite cement CC2 filled abundant primary porosity after compaction, especially in grain-dominated facies. CC2 composition is consistent with precipitation in an environment flushed by seawater (Moore, 2001) (Table 2). Those alterations affecting the Benassal Fm limestones from the replacement stage until uplift are described in detail in the following sections.

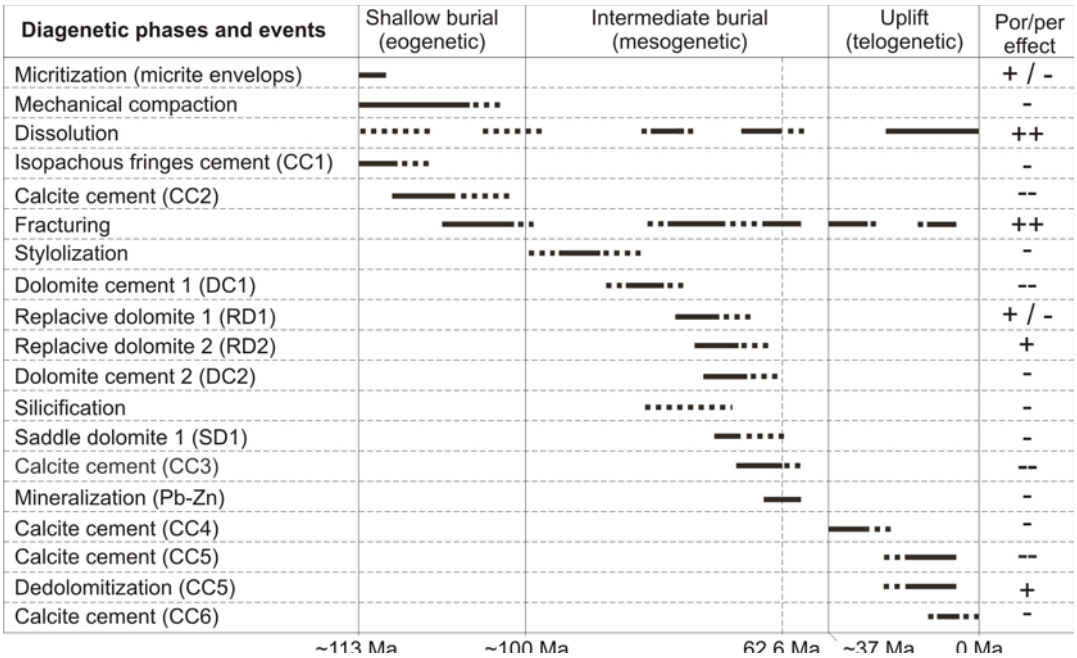


Figure 15: Paragenetic sequence of the Benassal Formation showing the relative timing of most important diagenetic alterations. Vertical dashed line indicates the emplacement of the MVT deposits in the Maestrat Basin (62.6±0.7 Ma; Grandia et al., 2000). Note that the diverse fracturing events, as well as dissolution events, appear all in the same line.

### 5.1.1 Burial dolomitization

Following the early calcite cementation and compaction, dolomite cement DC1 destroyed most of the remaining pore space in grain-dominated facies, which strongly controlled the subsequent host rock replacement process (Fig. 5 and 14). DC1 is interpreted to be the initial stage of dolomitization as indicated by: (1) the coexistence of DC1 with dolomite RD1 replacing matrix, grains, and bioclasts in limestones next to the dolomitization front; (2) the petrographic characteristics of DC1 resembling that of matrix replacive dolomite; and (3) the overlap in $\delta^{18}$O values between DC1 and RD1.

Preserved fabrics in RD1 crystal mosaics indicate that host limestone replacement took place after mechanical compaction, fracturing and stylolitization (Fig. 6), and thus during burial. RD1 represents the product of the bulk of the dolomitization (up to 70%), being the mimetic texture characteristic throughout the Benicàssim area. The replacement resulted in very tight RD1 crystal mosaics with only minor intercrystalline porosity, suggesting a partial inheritance of the precursor host limestone fabric (Martín-Martín et al., 2010) (Fig. 6). Despite the significant increase in DC1 in limestones located in the vicinity of the dolomitization front, this lithological boundary is dominantly sharp and separates the host limestone from completely dolomitized rocks. Therefore, the host limestone replacement is always complete (i.e., there are not partially dolomitized limestones), presumably related to crystal growth kinetics (Sibley et al., 1994).

The occurrence of RD1 relics in the core of dolomite RD2 crystals indicates a neomorphic recrystallization of the former (Fig. 7). Additional petrographic data suggesting recrystallization include (Gregg, 2004): (1) coarsening of crystal size and tendency to unimodal size distribution; and (2) homogenous luminescence character. Neomorphic recrystallization of replacive dolomites commonly results from successive diagenetic fluids until a more stable dolomite is formed (e.g. Land, 1980; Gregg and Shelton, 1990; Kaczmarek and Sibley, 2014). This is supported by the depleted $\delta^{18}O$ values measured in RD2 compared to RD1 crystals (Fig. 11). However, recrystallization from RD1 to RD2 is not associated with a significant increase in dolomite stoichiometry (Table 1), which suggests that neomorphism may have been driven by changes in crystal size reducing the surface energy (Ostwald ripening; e.g. Gregg and Shelton, 1990). Although RD2 is volumetrically much less significant than RD1, the increase in intercrystalline porosity associated with neomorphism probably increased the permeability of dolostones at time of dolomitization as well (Warren 2000; Gregg, 2004; Figs. 7 and 14).

Petrographic observations indicate that the replacement of the Benassal Fm occurred after stylolite formation and prior to MVT mineralization (Figs. 6 and Fig. 14). Bedding-parallel stylolites are reported to form between 300 and 800 m of burial depth in limestones (Dunnington, 1967; Nicolaides and Wallace, 1997; Ebner et al., 2008), and somewhat higher burial in dolostones due to their greater resistance to dissolution (Mountjoy and Amthor, 1994; Duggan et al., 2001). Assuming that stylolitization of the Benassal Fm initiated at an intermediate depth of the above reported range, the replacement of the host rock may have taken place between ˜500 m and the emplacement of the MVT (62.6±0.7 Ma; Grandia et al., 2000), which correspond to ˜750 m depth according to the burial curves by Martín-Martín et al. (2010) (Fig. 16). This burial range corresponds to a time span between ˜100 Ma (Cenomanian) and ˜63 Ma (Danian, and thus likely during the Late Cretaceous post-rift stage of Salas et al. (2001). Alternatively, the replacement of the Benassal Fm and the formation of the MVT deposit could represent a continuous process occurring within a relatively short period of time. In this case, dolomitization would have taken place around the onset of the Paleocene (66 Ma) and the time of MVT emplacement (62.6 Ma), and thus at burial depths close to 750 m (Fig. 16).

Dissolution of the remaining bioclasts, during the late stage or soon after the replacement process, produced abundant molds and significantly enhanced porosity in dolostones (Fig. 8). Thin and clear dolomite rim overgrowths (DC2) precipitated after dissolution (i.e. overdolomitization), which slightly reduced the newly created pore system. The reported sequence (replacement by dolomite, dissolution of undolomitized bioclasts and dolomite cementation) is typically observed in other dolomitized successions worldwide (e.g. Sun and Esteban, 1994; Machel, 2004; Wilson et al., 2007). The resulting DC2 planar crystal mosaic had the best reservoir quality at the time of dolomitization with occasional very well connected polyhedral pores (see Wardlaw, 1976) (Fig. 8). The dolomite planar crystal texture is dominant in thin (few meters thick) stratabound dolostone bodies located between tight unreplaced limestones, suggesting that they were preferential path ways for successive dolomitizing fluids.

Replacive dolomites (RD1 and RD2) and dolomite cement DC2 have $^{87}Sr/^{86}Sr$ signatures higher than those of the host limestones and consistent with a Late Cretaceous seawater signature (Fig. 12). Moreover, the relatively high Fe content (up to 3 wt%) of RD1, RD2 and DC2 suggests that the dolomitizing fluids interacted with siliciclastic rocks (Table 1). The most probable sources of radiogenic strontium, as well as Fe, are the underlying Permian-Triassic red beds and the metamorphic Paleozoic basement, which are in lateral contact with the Benassal Fm along the Benicàssim fault (Fig. 2).

### 5.1.2 Burial corrosion, carbonate cementation and MVT mineralization

Replacive dolomites and dolomite rim overgrowths are corroded, and thus postdated, by burial dissolution (Figs. 9 and 15). Corrosion was most likely related to the circulation of hot acidic fluids preceding the emplacement of the MVT deposits (e.g. Gregg, 2004). In this scenario, corrosion would have taken place during the extensional phase registered at the onset of the Paleocene (Grandia et al., 2000). Dissolution brines were focused along faults and fractures, and then through the dolostone matrix along the crystalline pore system and bedding-parallel stylolitic porosity (Fig. 9C-E). Frequently, sets of horizontally aligned vugs resulted from the enlargement of the stylolite pore system, reaching up to 1-m long in the proximity of most important faults (Martín-Martín et al., 2012b) (Fig. 9). The opening of stylolites occurred exclusively in dolostones due to their higher porosity/permeability matrix and higher brittleness compared to the host limestones.

Following dissolution, saddle dolomite SD1 and blocky calcite CC3 destroyed most of this vuggy porosity in dolostones (Fig. 9). SD1 lining stylolitic porosity is more frequent next to faults where it forms sets of horizontal saddle dolomite infillings (Fig. 9C). Most of these vugs or dissolution enlarged stylolites typically show a SD1 pore-lining and a CC3 infilling (Fig. 9D). CC3 filling mesovugs frequently engulfs dolostone clasts (i.e. floating clast hydraulic breccias), supporting the circulation of overpressured fluids through faults and stylolite conduits. In the Benicàssim area, however, saddle dolomite is volumetrically not significant and other typical hydrothermal textures like zebra dolomites (e.g., Davies and Smith, 2006; Swennen et al., 2012; Morrow, 2013) are generally absent.

Saddle dolomite SD1 and calcite cement CC3 from the Racó del Moro outcrop (Fig. 2) show $^{87}Sr/^{86}Sr$ ratios similar to those of replacive dolomites, which suggest that they precipitated from similar fluids that are consistent with Late Cretaceous seawater (Fig. 12). However, significantly higher $^{87}Sr/^{86}Sr$ values are recorded in SD1 and CC3 from the Campello mine (Gomez-Rivas et al., 2014), denoting the occurrence of more radiogenic brines in areas close to fault zones. The relatively high Fe content of saddle dolomite and, especially of CC3, supports the interaction of mineralizing fluids with subsurface Fe-rich rocks (Table 1 and 2).

Fluid inclusion homogenization temperatures (up to 190ºC) measured in post-replacement calcite cement CC3 from the Campello mine (Fig. 2) suggest that the highest temperature recorded in the Benicàssim area is most likely associated with the formation of the MVT sulfide deposits (Fig. 13). Moreover, highly depleted oxygen isotopes and elevated $^{87}Sr/^{86}Sr$ values of CC3 support that they precipitated from a hot, probably hydrothermal, radiogenic fluid (Fig. 12). Dolomite cementation accompanied or followed by precipitation of open-space-filling calcite cements is characteristic of carbonate-hosted sulfide deposits worldwide (Gregg, 2004). MVT deposits hosted in dolostones replacing the Lower Cretaceous limestones are frequent in the Maestrat Basin (Michel, 1974; Grandia, 2001; Grandia et al., 2003) (Fig. 1).

### 5.1.3 Carbonate cementation during uplift and subaerial exposure

Calcite cement CC4 is characterized by lower content in Fe2+, Mn2+, and Sr2+ compared to the burial calcite CC3, suggesting less interaction with basinal fluids and/or mixing with meteoric fluids (Table 2). Calcite cement CC4 occurs mostly in vertical fractures

indicating a close relationship with tectonic deformation during the Alpine orogeny or even the Neogene extension. The $^{87}Sr/^{86}Sr$ signature of CC4 is very similar to that of the host limestone, which suggests high rock/fluid interaction and/or inheritance from the former.

Calcite cement CC5, which includes calcitized dolomite, formed from predominantly meteoric fluids as indicated by the overall low content in Fe and Mn, non-luminescent character and depleted $\delta^{13}C$ (see Moore, 2001) (Fig. 8 and Fig. 10; Table 2). CC5 stable isotope values tend to be distributed along the meteoric calcite line (Lohmann, 1988), supporting formation in a diagenetic environment flushed by meteoric waters with variable contribution of soil gas (weathering). Such environment is most likely related to uplift and subaerial exposure, and thus dominant during the Neogene extension stage or younger times. Dolostones were preferentially cemented by CC5 compared to limestones due to their fracture network and higher porosity and permeability (Fig. 14). Some of these structures correspond to subseismic-scale faults reactivated after the replacement stage, as indicated by the presence of breccias made of dolomite clasts highly cemented by CC5 (Fig. 4). CC5 filled most of the intercrystalline porosity generated during the dolomitization process, and thus is the main reason for reservoir quality destruction in the studied rocks. CC5 preferentially cemented DC2- and RD2-dominated dolomite textures due to their higher pore connectivity at time of cementation, which may explain the nowadays higher porosity/permeability values in RD1-dominated samples (Fig. 14). Calcitization of dolomites (dedolomitization) and associated leaching preferentially occurred in fault zones and fractures. This is especially evident where the Campello and the Benicàssim seismic-scale faults cross-cut each other (Mortorum Hill) (Fig. 2).

The late episode of cementation is represented by the calcite cement CC6, which precipitated in a shallow diagenetic environment, in the vadose or phreatic zone, as indicated by its dominant gravitational texture (see Moore, 2001) (Fig. 10). CC6 stable isotope composition supports its formation from meteoric waters with high rock-water interaction (Fig. 11). Moreover, dolomite bands in CC6 show variable but elevated Na content, suggesting inheritance from the host dolostones. The above mentioned textural and analytical data inidcates that CC6 is most probably a speleothem (micro) formed in an oxic, vadose environment similar to those described by Alonso-Zarza and Martín-Pérez (2008).

## 5.2 Evidence of hydrothermal dolomitization

Fractionation of oxygen isotopes between carbonate minerals and fluids during precipitation is strongly dependent on temperature (e.g., Moore, 2001; Allan and Wiggins, 1993) thus the negative oxygen isotopic composition of replacive and cement dolomites is most likely indicative of high-temperature formation fluids. Accordingly, the progressively lighter oxygen isotopic composition from DC1 to RD1, and from RD1 to RD2 (Fig. 11), can be attributed to a progressive increase in fluid temperature during precipitation.

Fabric-retentive dolomite textures have been suggested to indicate precipitation at low temperatures (Machel, 2004). However, the replacement of the Benassal Fm limestones likely occurred at temperatures exceeding 80ºC as suggested by: (1) non-planar textures (Gregg and Sibley, 1984); (2) homogenous CL dull red color (Warren 2000); and (3) depleted $\delta^{18}O$ values (Allan and Wiggins, 1993). Carbon-oxygen isotope model curves calculated in terms of fluid-rock interaction are consistent with precipitation of replacive dolomite between 80 and 110ºC (Gomez-Rivas et al., 2010a, 2014). In agreement with this data, homogenization temperatures between 100 and 155ºC have been reported from dolostones replacing Aptian rocks elsewhere in the Maestrat Basin (Grandia, 2001; Nadal, 2001) (Fig. 13). Fluid inclusion data from saddle dolomite reported in the literature yielded temperatures above 60-80ºC in all cases, reaching maximum values around 160ºC (Sptl and Pitman, 1998). Therefore, the overlapping between replacive dolomite (RD1 and RD2) and saddle dolomite SD1 $\delta^{18}O$ values may suggest that all formed from similar high-

temperature fluids. A geothermal gradient of 30-35ºC/km was estimated by subsidence analysis for the Early Cretaceous rifting period of the Maestrat Basin (Caja et al., 2009). Decompacted subsidence curves indicate that the dolomitization reported from the study area occurred at burial depths of less than 1000 m (Fig. 16), and thus the maximum temperature reached by the dolomitized host rock due to burial would have been below 60ºC if other alternative heat sources are not invoked (Martín-Martín et al., 2010, 2013). However, textural and analytical data reported above indicate that the replacement of the Benassal Fm occurred at higher temperatures than those presumably reached by the host carbonates under the aforementioned geothermal gradient, indicating a hydrothermal dolomitization process (Gomez-Rivas et al., 2010a, 2014; Martín-Martín et al., 2010, 2013). Similar high-temperature replacement processes occurring at relatively shallow burial depths are well described in the literature (Gregg, 2004; Davies and Smith, 2006; López-Horgue et al., 2010).

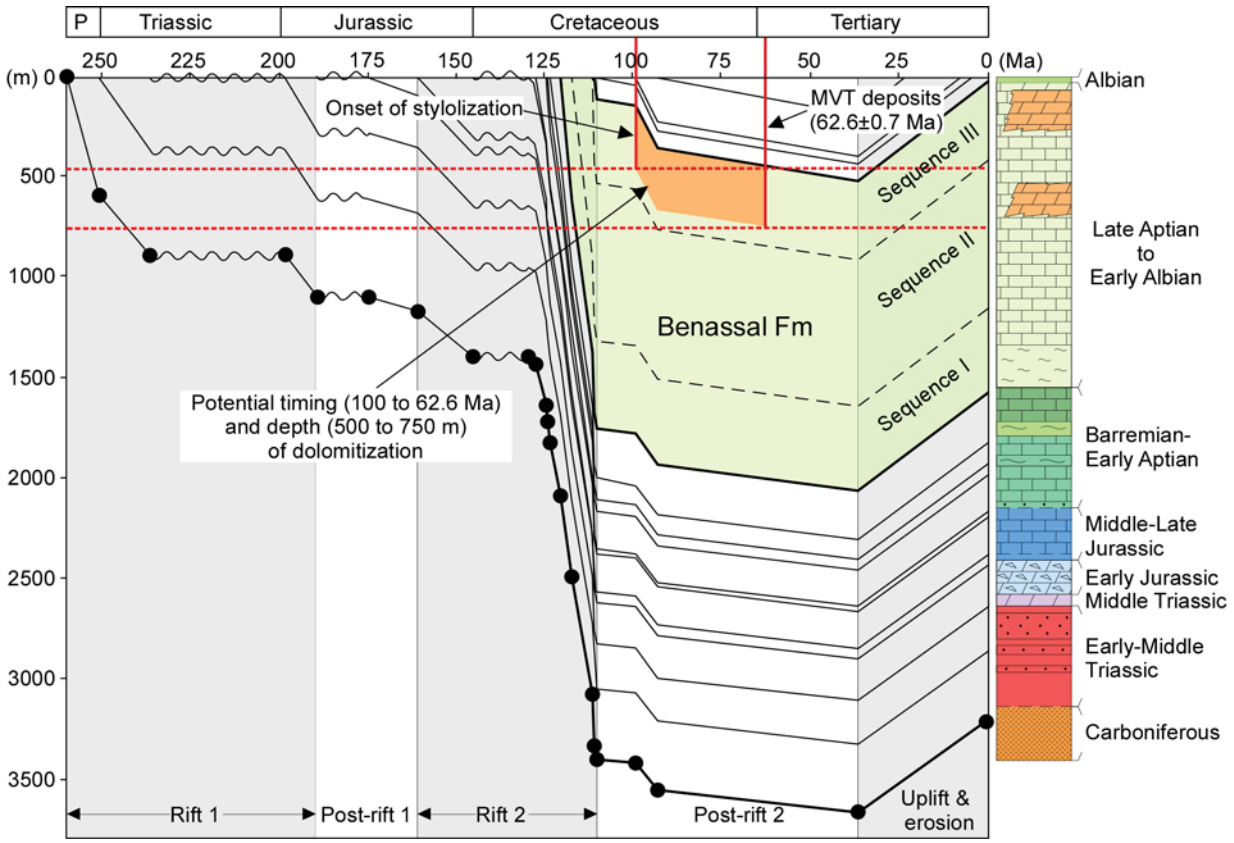


Figure 16: Mesozoic decompacted subsidence curves showing the most probable time and burial depth (orange area) for the upper stratabound dolostone body of the Benassal Fm (modified from Martín-Martín et al., 2010). The earliest replacement time is limited by the onset of the stylolitization (300-500 m), and the latest time corresponds to the emplacement of the MVT deposits in the Maestrat Basin (62.6±0.7 Ma; Grandia et al., 2000). The dashed red line denotes the inferred maximum burial depth at which dolomitization took place. Undulating lines correspond to gaps (erosion or non-deposition). Rift and post-rift cycles interpreted according to Salas et al. (2001).

Several high-temperature peaks occurring during Mid-Late Cretaceous have been reported in the Penyagolosa sub-basin (Fig. 1), supporting the hypothesis of a regional-scale hydrothermal fluid circulation at that time (Martín-Martín et al., 2013; Corbella et al., 2014; Gomez-Rivas et al., 2014). Dated processes involving high-temperature fluids include the formation of Hg-Sb-bearing ore deposits (140-180ºC) during Santonian at 85±3 Ma (Tritlla and Solé, 1999; Tritlla and Cardellach, 2003), and the development of high-temperature/low-pressure very low-grade metamorphism in Permian-Triassic rocks (300ºC) between Barremian (127±3 Ma) and Turonian (93±3 Ma) Martín-Martín et al.,

2005, 2009). The origin of these and other coeval phenomena reported in the area have been related to the thermal event taking place in the NE of the Iberian Plate during the Mid Cretaceous (Salas et al., 2005), coinciding with a period of rapid subsidence rates concomitant with the opening of the Bay of Biscay and the consequent counter clock wise of the Iberian Plate (Fig. 16). This thermal event is age-equivalent with that registered in the Basque Cantabrian Basin (López-Horgue et al., 2010; Dewit et al., 2012; López-Cilla et al., 2012; Nader et al., 2012; Shah et al., 2012; Swennen et al., 2012), suggesting that the hydrothermal dolomitization reported in both areas are most likely synchronous and related to the same large-scale geodynamic event.

## 5.3 Source of magnesium and dolomitization mechanism

Large-scale dolomitization processes require large volumes of magnesium in order to completely replace the host limestone (e.g., Land, 1985; Machel, 2004; Davies and Smith, 2006; Warren, 2006). The hypothesis of the magnesium origin in burial dolomitization are frequently difficult to corroborate using geochemical data, but is better constrained by means of mass-balance calculations (e.g., Reinhold, 1998; Gomez-Rivas et al., 2014). Diverse sources of magnesium have been claimed to be potentially involved in dolomitization processes (e.g., Qing and Mountjoy, 1994; Davies and Smith, 2006).

Considering the new analytical data reported here, the most likely sources of magnesium for the replacement of the Benicàssim dolostones are Cretaceous evolved seawater and basement fluids or a mixture of both (Gomez-Rivas et al., 2014). A source related to Upper Cretaceous seawater, or concentrated seawater, is fully consistent with the $^{87}Sr/^{86}Sr$ ratio of matrix replacive dolomites and saddle dolomites (Fig. 12). Moreover, the infiltration of such marine brines into deeper levels along the seismic-scale basement faults is compatible with the structural setting of the study area (Fig. 17), and may explain the relatively high Fe and Mn content in replacive dolomites. However, it is noteworthy that the absence of calcium sulphate minerals in the study area may argue against highly evaporated seawater. The strong radiogenic signature of saddle dolomite and calcite cement CC3 in the MVT site may suggests mixing of seawater with deep hydrothermal fluids (Gomez-Rivas et al., 2014). The presence of such fluids is also supported by the high temperature products reported from the Penyagolosa sub-basin and documented above: (i) MVT mineralization, (ii) Hg-Sb bearing deposits, and (iii) very low-grade metamorphism in Permian-Triassic rocks. The most likely scenario is that seawater invaded the sedimentary pile from the west where the Lower Cretaceous deposits onlap the Paleozoic basement in the Desert de les Palmes Ranges High and from the south where the same deposits onlap the València High.

Mass-balance calculations indicate that the source of the Mg-rich fluids needed for the replacement of the Benassal Fm limestones has to be considered at the regional scale (Corbella et al., 2014; Gomez-Rivas et al., 2014). This is consistent with the existence of several case studies of stratabound dolostones hosting MVT deposits in the Lower Cretaceous succession of the Penyagolosa sub-basin (Michel, 1974; Grandia, 2001) (Fig. 1 and 17). Moreover, hydrothermal events causing dolomitization and mineralization at regional scale are the most plausible origin of the vast amount of fluid needed for such processes to take place (e.g. Gregg, 2004; Saller and Dickson, 2011).

The huge volumes of fluid required to form the Benicàssim dolostones rule out potential individual small-scale fluid sources (Gomez-Rivas et al., 2014). However, mixing of Upper Cretaceus seawater with Lower Cretaceous formation waters and/or Upper Triassic-Early Jurassic post-evaporite residual brines are possible, especially if a basin-scale fluid circulation is assumed. In addition, burial compaction and subsequent dewatering of Aptian marly deposits may represent a potential source of Mg2+ if mixed with a more radiogenic fluid (Fig. 12). Late Triassic (Keuper facies) and Early Jurassic (Lias) evaporites are mostly eroded in the study area but are recognized from well cores to form thick subsur-

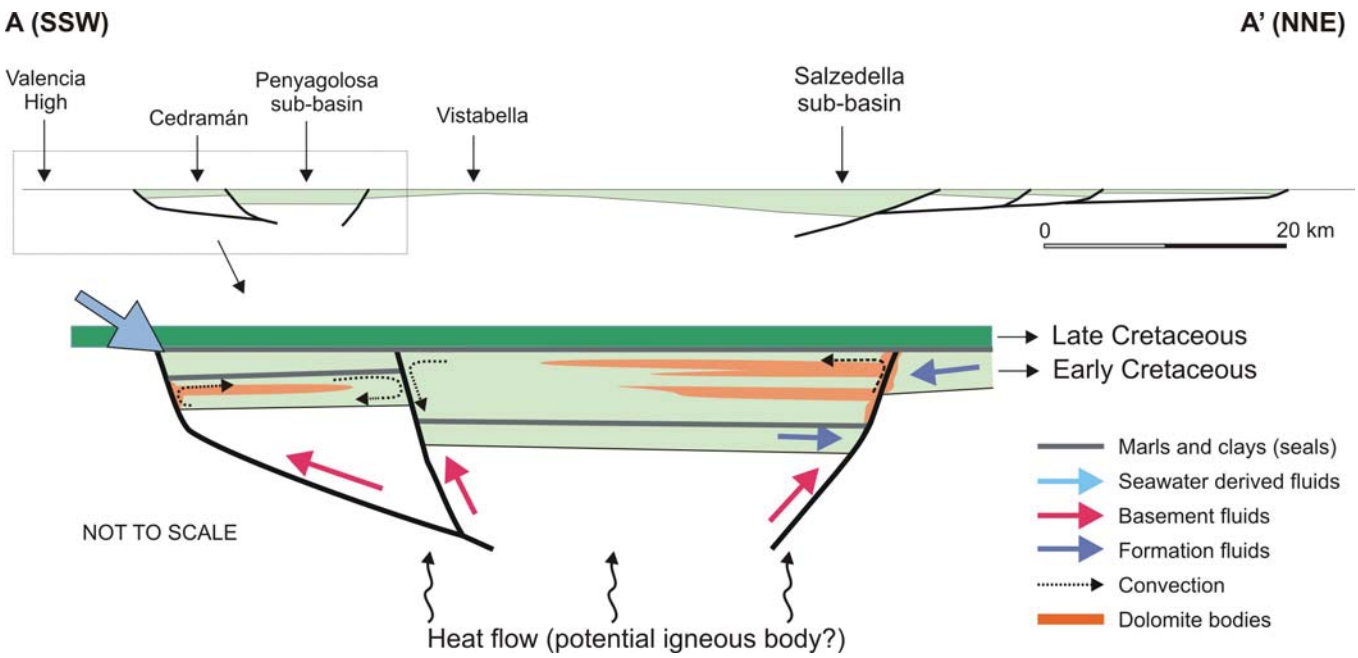


Figure 17: (A) Synthetic structural cross-section of the Maestrat Basin restored at the base of the Albian-Cenomanian post-rift succession (modified from Salas et al., 2001) (see figure 1 for location). (B) Conceptual integrative model for the formation of the stratabound dolostones of the Benicàssim area based on field observations, analytical data and geochemical modeling (Gomez-Rivas et al., 2014), reactive transport modeling (Stafford et al., 2009; Corbella et al., 2014), fluid and heat flow numerical simulations (Gomez-Rivas et al., 2010b), and previous studies of fault-related dolostones in the Maestrat Basin (Grandia, 2001; Nadal, 2001).

face deposits elsewhere in the Maestrat Basin (Lanaja, 1987; Ortí and Pérez-López, 1994). Based on their $^{87}Sr/^{86}Sr$ values, these evaporites have been claimed to be the origin of the Mg-rich brines for the dolomitization for the Late Jurassic fault-related dolomites in the Maestrat Basin (Nadal, 2001), and it could be the case of the Aptian dolomites in the Benicàssim area as well. However, the enormous amount of evaporites that would have to be dissolved in order to account for such dolostone volume clearly discards these brines if other additional sources are not involved (Fig. 12).

Together with a source of magnesium, there must have been a major driving mechanism to mobilize the magnesium-rich fluid into the host limestones. Such a mechanism has to explain the long lateral continuity of the dolomitized bodies and its close association with faults. Taking into account the structural setting of the Benicàssim area, the elemental and isotopic composition of dolostones, and the hydrothermal character of the dolomitizing fluid, the most likely mechanism is thermal convection (Gomez-Rivas et al., 2010b, 2014; Martín-Martín et al., 2010, 2013; Corbella et al., 2014). Thermal convection may supply higher fluid and heat flow rates for dolomitization than other possible mechanisms (Kaufman, 1994; Wilson et al., 2001; Davies and Smith, 2006; Gasparrini et al., 2006), and is in agreement with fluid flow, heat flow and reactive transport numerical simulations applied to the Benicàssim area (Gomez-Rivas et al., 2010b; Corbella et al., 2014). The source of the abnormal heat flow, and thus hydrothermalism, is most likely associated with the Mid-Late Cretaceous thermal event caused by a deep igneous intrusion under the eastern Iberian Plate (Salas et al., 2005). In the study area, heat and fluid flow convection was probably enhanced by the presence of seismic-scale basement faults that formed a perpendicular fracture network with the regional fault system. Specifically, the SSW-NNE Benicàssim fault connected the Desert de les Palmes High with the NW-SE Campello fault, both faults considered to be the preferential conduits for the dolomitizing fluids.

## 5.4 Controls on stratabound dolostone formation

Dolostone distribution through the Benicàssim area indicates that the replacement of the Benassal Fm limestones was primarily controlled by the regional fault system (Martín-Martín et al., 2013; Gomez-Rivas et al., 2014). Dolostones bodies appear in close spatial association with both the NW-SE-trending (Campello and Juvellús) and the NNE-SSW-trending (Benicàssim) fault systems, mainly in the hanging wall blocks, indicating that these seismic-scale structures acted as major conduits for dolomitizing fluids (Fig. 2). The association of dolostones and MVT deposits with the Campello fault evidence that it represented a common conduit channeling successive dolomitizing and mineralizing fluids (e.g. Gregg, 2004; Davies and Smith, 2006). In this regard, the occurrence of more radiogenic burial carbonate cements in the vicinity of the Campello fault supports that it was a preferential feeding point of subsurface fluids. A similar close relation between dolostone geobodies and faults have been extensively reported in the literature (e.g., Duggan et al., 2001; Wilson et al., 2007; Davies and Smith, 2006; López-Horgue et al., 2010; Shah et al., 2010; Sharp et al., 2010; Di Cuia et al., 2011; Ronchi et al. 2012).

Despite the extensive outcrop of dolostone geobodies, their exact geometry in the fault zones are hardly observed throughout the Benicàssim area due to the post-dolomitization overprint of the Alpine and Neogene deformation events (Martin-Martín et al., 2013). In particular, the Neogene extension caused the offset of most dolostone bodies facilitating their fossilization by Quaternary deposits along the fault scarps (Fig. 2). At Benicàssim, dolostone bodies are dominantly stratabound and extent up to ∼4 km away from the feeding faults, which denotes a strong lateral flow of dolomitizing fluids along the country rock (Martín-Martín et al., 2010, 2013). Field observations suggest that the circulation of dolomitizing and mineralizing brines away from major faults was focused along minor faults (subseismic-scale) that were repeatedly reactivated during the evolution of the study area (Fig. 2). For example, these minor faults fed the dolostone bodies through fractures, joints and stylolites, all discontinuities being preferential sites for post-replacement burial carbonate cements SD1 and CC3.

The presence of relict limestones (i.e., stringers) within the stratabound dolostone body suggests that, together with the structure, there must be other controls that played a role in the dolomitization process. At the Racó del Moro, the reported unreplaced beds are mostly tight limestones consisting of mud-dominated facies with very low porosity and permeability (Fig. 2 and 3) (Martín-Martín et al., 2013). This strata are characterized by nodular bedding containing networks of anastomosing stylolites that acted as dolomitizing fronts, and thus as barriers to flow, during the replacement (Fig. 4). These low porosity and permeability stylolitic-rich limestones enhanced lateral flow and thus the stratabound geometry of the dolostones away from the feeding faults (Martín-Martín et al., 2013). These structural, diagenetic and depositional controls facilitating the replacement of specific limestones beds are key factors to define mechanical stratigraphy, which in terms have been claimed to control the formation of stratabound dolostones in the Basque-Cantabrian Basin (Dewit et al., 2014).

Mimetic textures in replacive dolomite crystal mosaics evidence that grainy facies (e.g., peloidal grainstones, bioclastic packstones, and orbitolinid rudstones) were preferentially replaced, indicating that they were the most permeable layers at time of dolomitization. This is supported by (i) higher porosity and permeability values in dolomite-cemented peloidal and orbitolinid grainstones from the base of the Benassal Fm (Fig. 14), and (ii) the fact that there are very few unreplaced grainstones within the dolostone bodies. At the Racó del Moró, the dolostone body include the maximum flooding surface, suggesting that dolomitizing fluids circulated along and replaced the grainy facies of the transgressive and regressive tracks until they reached the lower permeability outer ramp muddy facies. Moreover, the presence of unreplaced oolitic grainstone facies highly cemented by early diagenetic calcite in the vicinity of the dolostone bodies suggests that early marine cementation destroyed most of the porosity and prevented dolomitizing fluids to flow through

them (see Martín-Martín et al., 2013).

At the thin section scale, petrography indicates that several factors may influence the replacement of the host rock matrix. Firstly, the dolomitization seems to expand from the dolomite cement DC1 towards the micrite matrix and/or micritized grains, being the more stable calcite cement the last component to be replaced (Fig. 5C and D). It is believed that the dolomite cement DC1 acted as a seed, enhancing the dolomitization of the whole rock and overpassing some of the limiting factors that control the replacement of large volumes of rock (Land, 1985; Whitaker et al., 2004; Jones et al., 2011). Secondly, the replacement may have been enhanced by the occurrence of cm- to mm-scale cracks that propagate along, and connect the edges of, the coarser skeletal components forming conduits for fluid flow at time of alteration.

# 6 Conclusions

The petrological and geochemical data reported in this study indicate that the Benassal Fm dolostones exhibit a burial paragenesis consisting in replacement of the host limestone, precipitation of clear dolomite overgrowths, burial corrosion, and carbonate cementation prior to MVT sulphide mineralization. The initial stage of the replacement consisted in the precipitation of dolomite cement in the intergranular porosity of the grain-dominated facies, which strongly controlled the subsequent dolomitization of the host rock. The bulk of the dolostone is formed by a replacive non-planar to planar-s dolomite crystal mosaic with very low porosity. Neomorphic recrystallization of the later occurred in relation to successive fluid flow along the higher permeability zones. The reported replacement sequence is associated with a decrease in the oxygen isotopic composition of dolomite, interpreted to result from progressively higher temperature fluids. Petrographic and geochemistry data suggests that the dolomitization took place by hydrothermal fluids, likely at temperatures exceeding 60-80ºC. The replacement occurred after stylolitization and at relatively shallow burial (between 500 and 750 m) during the Late Cretaceous post-rift stage of the Mesozoic Iberian Rift System.

Dolostone distribution through the Benicàssim area indicates that the replacement of the Benassal Fm limestones was primarily controlled by seismic-scale basement faults that operated as feeding points for the dolomitizing brines. The fluid circulation, and thus the replacement, was enhanced by the intersection of two seismic-scale fault systems (trending NW-SE and NNE-SSW). We envisage Mg-rich fluids, most likely Cretaceous seawater-derived brines, that were heated and slightly enriched in radiogenic strontium and iron during circulation through the Paleozoic basement and/or Permo-Triassic red beds, which are in lateral contact with the Benassal Fm by fault. High temperature Mg-rich fluids were later channeled upwards along the above mentioned seismic-scale faults and laterally through the higher permeable units of the host rock succession. Lateral fluid flow through the bedding was most probably enhanced by the overlying Escucha Fm clays, which is considered the former seal. Successive fluid flow induced the recrystallization of the initial matrix replacive dolomite (i.e., RD1 to RD2), as well as the subsequent formation of clear dolomite overgrowths (overdolomitization). The transformation of RD1 to DR2 crystal mosaics lead to an increase in the reservoir quality of the dolostone bodies.

Once in the host limestones and away of the fault zones, dolomitization brines preferentially circulated through small-scale faults, fractures, and grainy facies. By contrast, low-permeability and highly stylolitized muddy facies (mudstones and wackestones) acted as barriers for the dolomitizing fluids, enhancing the lateral flow and the stratabound dolostone distribution. These tight beds occasionally individualize thin dolostone bodies that might constitute high permeable conduits at time of alteration.

After the replacement stage, as typically reported in other case studies of hydrothermal dolomites, reservoir quality considerably increased in dolostones by burial corrosion, which was closely associated with the circulation of acidic fluids derived from the em-

placement of the Mississippi Valley-Type deposits. Major faults acted as feeding points of acidic and overpressured fluids that penetrate the dolostone matrix along outcrop-scale faults, fractures, and parallel to bedding stylolites. Saddle dolomite and ore-stage calcite cement filled most of the newly created meso- to micro-porosity. Precipitation of post-replacement, open-space-filling, calcite cement occurred at temperatures ranging between 120 and 190℃.

Reservoir quality of dolostones was mostly destroyed by the pervasive pore-occluding calcite cementation that took place during the uplift and subaerial exposure (Alpine compression and Neogene extension). The precipitation of calcite resulted from the circulation of meteoric-derived fluids through the well-connected intercrystalline pore system of dolostones, which otherwise formed a good hydrocarbon reservoir in the subsurface. Dolomite calcitization (dedolomitization), which is associated with the the circulation of meteoric fluids, was more intense in those dolostone bodies located in the intersection between major faults where discrete Fe-oxide deposits were originated. The presence of this mineralization reinforces the hypothesis that the above mentioned regional faults sourced Fe-rich fluids during the replacement stage, repeatedly acting as major fluid conduits during the subsequent geodynamic evolution of the study area.

# Acknowledgements

This study was developed under the ExxonMobil FC2 Alliance (Fundamental Controls on Flow in Carbonates). The authors wish to thank ExxonMobil Production Company and ExxonMobil Upstream Research Company for providing funding. The views in this article by Sherry L. Stafford are her own and not necessarily those of ExxonMobil. This research was supported by the Sedimentary Geology Research Group of the Generalitat de Catalunya (2014SGR251). We would like to thank Andrea Ceriani and Paola Ronchi for their critical and valuable reviews, and Associated Editor Piero Gianolla for the editorial work.

# References cited

- Allan, J.R., Wiggins, W.D., 1993. Dolomite reservoirs: Geochemical techniques for evaluating origin and distribution, Am. Assoc. Pet. Geol. Contin. Educ. Course Notes 36, Tulsa.
- Alonso-Zarza, A.M., Martín-Pérez, A., 2008. Dolomite in caves: Recent dolomite formation in oxic, non-sulfate environments. Castaar Cave, Spain. Sedimentary Geology 205, 160164.
- Bakker, R.J., 2003. Package FLUIDS 1. Computer programs for analysis of fluid inclusion data and for modelling bulk fluid properties. Chem. Geol. 194, 3-23.
- Bover-Arnal, T., Martín-Martín, J.D., Gomez-Rivas, E., Travé, A., Salas, R., Moreno-Bedmar, J.A., Tomás, S., 2009. Insights into the Upper Aptian carbonate succession of the South-Eastern Maestrat basin (E Iberia), in: Amorosi, A. (Ed.), 27th IAS Meeting of Sedimentologists, Medimond International Proceedings, Bologna, pp. 123-128.
- Caja, M.A., Salas, R., Marfil, R., Permanyer, A., 2009. Paleothermal constraints from diagenetic minerals recording high temperature conditions in a rift basin (Maestrat Basin, Iberian Range). J. Geoch. Expl. 101, 18.
- Cavailhes, T., Sizun J.-P., Labaume, P., Chauvet, A., Buatier, M., Soliva, R., Mezri, L., Charpentier, D., Travé, A., Gout, C., 2013. Influence of fault rock foliation on fault zone permeability: The case of deeply buried arkosic sandstones (Grès dAnnot, SE France). AAPG Bull. 97 (9), 1521-1543.
- Choquette, P.W., Pray, L.C. 1970. Geologic nomenclature and classification of porosity in sedimentary carbonates. AAPG Bull. 54, 207-250.
- Clavell, E., Berastegui, X., 1991. Petroleum geology of the Gulf of València, in: Spencer, M.A., (Ed.), Generation, Accumulation, and Production of Europes Hydrocarbons, Sp. Pub. Eur. Assoc. Petrol. Geosc., Oxford University Press, Oxford, pp. 355-68.

- Corbella, M., Gomez-Rivas, E., Martín-Martín, J.D., Stafford, S.L., Teixell, A., Griera, A., Travé, A., Cardellach, E., Salas, R., 2014. Insights to controls on dolomitization by means of reactive transport models applied to the Benicàssim case study (Maestrat Basin, eastern Spain). Petrol. Geosc. 20 (1), 41-54.
- Davies, G.R., Smith, L.B.J., 2006. Structurally controlled hydrothermal dolomite reservoir facies: An overview. AAPG Bull. 90, 1641-1690.
- Dewit, J., Huysmans, M., Muchez, P., Hunt, D.W., Thurmond, J.B., Vergés, J., Saura, E., Fernandez, N., Romaire, I., Esestime, P., Swennen, R., 2012. Reservoir characteristics of fault-controlled hydrothermal dolomite bodies: Ramales Platform case study, in: Garland, J., Neilson, J.E., Laubach, S.E. and Whidden, K.J. (Eds), Advances in Carbonate Exploration and Reservoir Analysis, Geological Society of London, Special Publications 370, London, pp. 83-109.
- Dewit, J., Foubert, A., El Desouky, H.A., Muchez, P., Hunt, D., Vanhaecke, F., Swennen, R., 2014. Characteristics, genesis and parameters controlling the development of a large stratabound HTD body at Matienzo (Ramales Platform, Basque-Cantabrian Basin, northern Spain). Mar. Petrol. Geol. 55, 6-25.
- Di Cuia, R., Riva, A., Scifoni, A., Moretti, A., Sptl, C., Caline, B., 2011. Dolomite characteristics and diagenetic model of the Calcari Grigi Group (Asiago Plateau, Southern Alps - Italy): an example of multiphase dolomitization. Sedimentology 58(6), 1347-1369.
- Duggan, J.P., Mountjoy, E.W., Stasiuk, L.D., 2001. Fault-controlled dolomitization at Swan Hills Simonette oil field (Devonian), deep basin west-central Alberta, Canada. Sedimentology 48, 301-323.
- Dunnington, H.V., 1967. Aspects of diagenesis and shape in stylolitic limestone reservoirs, in: Origin of Oil, Geology and Geophysics, Proceedings of the 7th World Petroleum Congress (vol. 2), pp. 339-352.
- Ebner, M., Koehn, D., Toussaint, R., Renard, F., Schmittbuhl, J., 2008. Stress sensitivity of stylolite morphology. Earth. Planet. Sci. Lett. 277, 394-398.
- Garcia, R., Moreno-Bedmar, J.A., Bover-Arnal, T., Company, M., Salas, R., Latil, J-L., Martín-Martín, J.D., Gomez-Rivas, E., Bulot, L.G., Delanoy, G., Martínez, R., Grauges, A., 2014. Lower Cretaceous (Hauterivian-Albian) ammonite biostratigraphy in the Maestrat Basin (E Spain). J. Iber. Geol. 40(1), 99-112.
- Gasparrini, M., Bechstdt, T., Boni, M., 2006. Massive hydrothermal dolomites in the southwestern Cantabrian Zone (Spain) and their relation to the Late Variscan evolution. Mar. Petrol. Geol. 23(5), 543-568.
- Gomez-Rivas, E., Corbella, M., Martín-Martín, J.D., Stafford, S. L., Teixell, A., Bons, P. D., Cardellach, E., 2014. Reactivity of dolomitizing fluids and Mg source evaluation of fault-controlled dolomitization at the Benicàssim outcrop analogue (Maestrat Basin, E Spain). Mar. Petrol. Geol. 55, 26-42.
- Gomez-Rivas, E., Corbella, M., Martín-Martín, J.D., Teixell, A., Cardellach, E., 2010a. Reactivity of dolomitizing fluids and evaluation of Mg sources in the Benicassim area (Maestrat Basin, E Spain). 72nd European Association of Geoscientists and Engineers Conference and Exhibition, Paper SPE 39497, Barcelona, 2831-2835.
- Gomez-Rivas, E., Stafford, S.L., Lee, A.G.K., Corbella, M., Martín-Martín, J.D., Teixell, A., 2010b. Flow patterns of dolomitizing solutions in a buried carbonate ramp the Benicassim case study (Maestrat Basin, NE Spain). 72nd European Association of Geoscientists and Engineers Conference and Exhibition, Paper SPE 39522, Barcelona, 2954-2959.
- Gomez-Rivas, E., Warber, K., Kulzer, F., Bons, P.D., Koehn, D., Martín-Martín, J.D., 2012. Structural evolution of the Benicàssim area (Maestrat basin, NE Spain): insights from fracture and vein analysis. Geogaceta 51, 79-82.
- Grandia, F., 2001. Origen, evolució i edat dels fluids associats a les mineralitzacions de Zn-Pb en carbonats cretàcics de la Conca del Maestrat (Castelló-Teruel), Unpublished PhD thesis, Universitat Autònoma de Barcelona, Barcelona.
- Grandia, F., Asmerom, Y., Getty, S., Cardellach, E., Canals, A., 2000. U-Pb dating of MVT ore-stagecalcite: implications for fluid flow in a Mesozoic extensional basin from Iberian Peninsula. J. Geoch. Explor. 69-70, 377-380.

- Grandia, F., Cardellach, E., Canals, A., Banks, D.A., 2003. Geochemistry of the fluids related to epigenetic carbonate-hosted Zn-Pb deposits in the Maestrat Basin, Eastern Spain: fluid inclusion and isotope (Cl, C, O, S, Sr) evidence. Econ. Geol. 98, 933-954.
- Gregg, J.M., 2004. Basin fluid flow, base-metal sulphide mineralization and the development of dolomite petroleum reservoirs, in: Braithwaite, C.J.R., Rizzi, G. and Darke, G. (Eds.), The Geometry and Petrogenesis of Dolomite Hydrocarbon Reservoirs, Geol. Soc. Lon. Sp. Pub. 235, London, 157-175.
- Gregg, J.M., Shelton, K.L., 1990. Dolomitization and dolomite neomorphism in the back reef facies of the Bonneterre and Davis Formations (Cambrian), southeastern Missouri. J. Sed. Petrol. 60, 549-562.
- Gregg, J.M., Sibley, D.F., 1984. Epigenetic dolomitization and the origin of xenotopic dolomite texture. J. Sed. Petrol. 54, 908-931.
- Haynes, F.M., 1985. Determination of fluid inclusion composition by sequential freezing. Econ. Geol. 80, 1436-1439.
- Jones, C.E., Jenkins, H.C., 2001. Seawater strontium isotopes, oceanic anoxic events, and seafloor hydrothermal activity in the Jurassic and Cretaceous. Am. J. Sci. 301, 112-149.
- Jones, G.D., Gupta, I., Sonnenthal, E., 2011. Reactive transport models of structurally controlled hydrothermal dolomite: Implications for Middle East carbonate reservoirs. GEO 2010 (9th Middle East Geosciences Conference). GeoArabia 16, 194-195.
- Kaczmarek, S.E., Sibley, D.F., 2007. A comparison of nanometer-scale growth and dissolution features on natural and synthetic dolomite crystals: implications for the origin of dolomite. J. Sediment. Res. 77, 424-432.
- Kaufman, J., 1994. Numerical models of fluid flow in carbonate platforms - implications for dolomitization. J. Sed. Res. 64 (Sect. A), 128-139.
- Lanaja, J.M., 1987. Contribución de la exploración petrolífera al conocimiento de la Geología de Espaa, IGME, Servicio de Publicaciones de Industria y Energía, Madrid.
- Land, L.S., 1980. The isotopic and trace element geochemistry of dolomite: The state of the art., in: Zenger, D.H., Dunham, J.B. and Ethingtin, R.L. (Eds.), Concepts and Models of Dolomitization, Soc. Econ. Pal. Min. Sp. Pub. 28, Tulsa, 87-110.
- Land, L.S., 1985. The origin of massive dolomite. J. Geol. Educ. 33, 112-125.
- Lapponi, F., Casini, G., Sharp, I., Blendinger, W., Fernandez, N., Romaire, I., Hunt, D., 2011. From outcrop to 3D modelling: a case study of a dolomitized carbonate reservoir, Zagros Mountains, Iran. Petrol. Geos. 17(3), 283-307.
- Laubach, S.E., Olson, J.E., Gross, M.R., 2009. Mechanical an fracture stratigraphy. AAPG Bulletin 93, 1413-1426.
- Lohmann, K.C., 1988. Geochemical patterns of meteoric diagenetic systems and their application to studies of paleokarst, in: James, N.P., Choquette, P.W., (Eds.), Paleokarst, Springer-Verlag, New York, pp. 58-80.
- Lomando A.J., Harris P.M., Orlopp D.E., 1993. Casablanca field, Tarragona Basin, offshore Spain: a karsted carbonate reservoir, in: Fritz, R.D., Wilson, J.L., Yurewicz, D.A., (Eds.), Paleokarst Related Hydrocarbon Reservoirs, Core Workshop 18 in New Orleans, SEPM 201-25, Tulsa.
- López-Cilla, I., Rosales, I., Najarro, M., 2012. Diagenesis in Lower Cretaceous platform carbonates of northern Spain (NW Cantabria): an example of multistage dolomitization and calcite cementation. Geofluids VII Abstract Book, Paris, pp. 205-208.
- López-Horgue, M.A., Iriarte, E., Schrder, S., Fernández-Mediola, P.A., Caline, B., Corneyllie, H., Frémont, J., Sudrie, M., Zerti, S., 2010. Structurally controlled hydrothermal dolomites in Albian carbonates of the Asón valley, Basque Cantabrian Basin, Northern Spain. Mar. Petrol. Geol. 27 (5), 1069-1092.
- Machel, H.G., 2004. Concepts and models of dolomitization: a critical reappraisal. Geol. Soc. Lon. Sp. Pub. 235, London, pp. 7-63.
- Martín-Martín, J.D., Gomez-Rivas, E., Bover-Arnal, T., Travé, A., Salas, R., Moreno-Bedmar, J.A., Tomás, S., Corbella, M., Teixell, A., Vergés, J., Stafford, S.L., 2013. The Aptian syn-rift carbonate succession of the southern Maestrat Basin (Spain): Facies architecture and fault controlled stratabound dolostones. Cretac. Res. 41, 217-236.

- Martín-Martín, J.D., Gomez-Rivas, E., Travé, A., Salas, R., Vergés, J., 2012a. Dolomías controladas por fracturas en carbonatos aptienses de la zona de Benicàssim (SE Cuenca del Maestrat): distribución y características petrográficas. Geogaceta 51, 19-22.
- Martín-Martín, J.D., Ameneiro, R., Gómez-Gras, D., Travé, A., 2012b. Macroporosity distribution in fault-controlled dolostones from the SE Maestrat Basin (Spain). Geofluids VII Abstract Book, Paris, 223-226.
- Martín-Martín, J.D., Travé, A., Gomez-Rivas, E., Sizun, J.P. Salas, R., Gómez-Gras. D., Vergés, J., 2010. Faultassociated dolomites in the Benicàssim area, Maestrat Basin, E. Spain Macro to microscale fluid flow in carbonates. 72nd European Association of Geoscientists and Engineers Conference and Exhibition, Paper SPE 39527, Barcelona, 2980-2984.
- Martín-Martín, J.D., Salas, R. Gómez-Gras, Zwingmann, H., 2009. K/Ar isotopic dating of very low-grade metamorphic and late diagenetic conditions during the Mesozoic rifting evolution of the Iberian Chain, Spain, in: Fiore, S., Belviso, C., Giannossi, M.L., (Eds.), XIV International Clay Conference (Italy), Micro et Nano: Scientae Mare Magnum, Associazione Italiana per lo Studio delle Argille. Book of Abstracts, pp. 236.
- Martín-Martín, J.D., Sanfeliu, T., Gómez-Gras, D., 2005. Mineralogía de arcillas cerámicas. El Permo-Trías de Castelló, Publicacions de la Universitat Jaume I (Athenea 13), Castelló de la Plana.
- Martínez, R., Grauges, A., Salas, R., 1994. Distribución de los ammonites del Cretácico inferior de la Cordillera Costera Catalana e Ibérica Oriental. Cuad. Geol. Iber. 18, 337-354.
- Michel, B., 1974. Contributions a l'étude des minéralisations plombo-zinciferes dans de Crétacé Inférieur du Maestrazgo, Unpublished PhD thesis, University of Nancy, France
- Moore, C.H., 2001. Carbonate reservoirs. Porosity evolution and diagenesis in a sequence stratigraphic framework, Developments in sedimentology 55, Elsevier.
- Moreno-Bedmar, J.A., Company, R., Bover-Arnal, T., Salas, R., Delanoy, G., Maurrasse, F.J.-M.R., Graugés, A., Martínez, R., 2010. Lower Aptian ammonite biostratigraphy in the Maestrat Basin (Eastern Iberian Chain, Easter Spain). A Tethyan transgressive record enhanced by synrift subsidence. Geol. Acta 8 (3), 281-299.
- Morrow, D.W., 2013. Zebra and boxwork fabrics in hydrothermal dolomites of northern Canada: Indicators for dilational fracturing, dissolution or in situ replacement? Sedimentology. doi:10.1111/sed.12094.
- Mountjoy, E.W., Amthor, J.E., 1994. Has burial dolomitization come of age? Some answers from the western Canada sedimentary basin, in: Dolomites: Purser, B., Tucker. M., Zenger, D. (Eds.), a Volume in Honour of Dolomieu, Inter. Assoc. Sedimentol. Spec. Publ. 21, pp. 203-229.
- Nadal, J., 2001. Estudi de la dolomitització del Juràssic superior-Cretaci inferior de la Cadena Ibérica oriental y la Cadena Costanera Catalana: relació amb la segona etapa de rift mesozoica, Unpublished PhD thesis, Universitat de Barcelona, Spain.
- Nader, F. H., López-Horgue, M. A., Shah, M. M., Dewit, J., Garcia, D., Swennen, R., Caline, B., 2012. The Ranero Hydrothermal Dolomites (Albian, Karrantza Valley, Northwest Spain): Implications on Conceptual Dolomite Models. Oil Gas Sci. Techn., Revue dIFP Energies Nouvelles, 67(1), 9-29.
- Nicolaides, S., Wallace, M.W., 1997. Pressure-dissolution and cementation in an Oligotropical limetone (Clifton Formation), Otway Basin, Australia, in: James, N.P., Clarke, J.A.D. (Eds.), Cool Water Carbonates, Soc. Econ. Petrol. Geol. Spec. Publ. 56, pp. 249-261.
- Ortí, F., Pérez-López, A., 1994. El Triásico superior del Levante. III Coloquio de Estratigrafía y Paleogeografía del Pérmico-Triásico de Espaa. Guía de Excursiones, Cuenca, 63 p.
- Qing, H., Mountjoy, E.W., 1994. Origin of dissolution vugs, caverns and breccias in the middle Devonian Presuile Barrier, host of Pine Point MVT deposits. Econ. Geol. 89, 858-876. Reinhold, C., 1998. Multiple episodes of dolomitization and dolomite recrystallization during shallow burial in Upper Jurassic shelf carbonates: eastern Swabian Alb, southern Germany. Sed. Geol. 121, 71-95.

- Roca, E., Guimerà, J., 1992. The Neogene structure of the eastern Iberian margin: structural constraints on the crustal evolution of the Valencia trough (western Mediterranian). Tectonoph. 203, 203-218.
- Roca, E., Guimerà, J., Salas, R., 1994. Mesozoic extensional tectonics in the southeast Iberian Chain. Geol. Mag. 131, 155-168.
- Ronchi, P., Masetti, D., Tassan, S., Camocino, D., 2012. Hydrothermal dolomitization in platform and basin carbonate successions during thrusting: A hydrocarbon reservoir analogue (Mesozoic of Venetian Southern Alps, Italy). Mar. Petrol. Geol. 29(1), 68-89.
- Salas, J., Caja, M.A., Mas, R., Martín-Martín, J.D., Mas, R., Permanyer, A., 2005. Mid-Late Cretaceous volcanism, metamorphism and the regional thermal event affecting the Northeastern Iberian Basins (Spain), in: Arnaud-Vanneau, A., Arndt, N., Zghal (Eds.), Global events during the quiet Aptian-Turonian superchron. Laboratoire de Géologie de lUniversité I de Grenoble, Geologie Alpine, Série Spéciale N 6, Grenoble.
- Salas, R., Casas, A., 1993. Mesozoic extensional tectonics, stratigraphy and crustal evolution during the Alpine cycle of the eastern Iberian basin. Tectonoph. 228(1-2), 33-55.
- Salas, J., Guimerà, J., Mas, R., Martín-Closas, A., Meléndez, A., Alonso, A., 2001. Evolution of the Mesozoic central Iberian Rift System and its Cainozoic inversion (Iberian chain), in: Ziegler, P.A., Cavazza, W., Robertson, A.H.F., Crasquin-Soleau, S., (Eds.), Peri-Tethyan Memoir 6: Peri-Tethyan Rift/Wrench Basins and Passive Margins. Mém. Mus. Natn. Hist. Nat. 186, Paris, pp. 145-185.
- Saller, A.H., Dickson, J.A.D., 2011. Partial dolomitization of a Pennsylvanian limestone buildup by hydrothermal fluids and its effect on reservoir quality and performance. AAPG Bull. 95(10), 1745-1762.
- Shah, M.M., Nader, F.H., Dewit, J., Swennen, R., Garcia, D., 2010. Fault-related hydrothermal dolomites in Cretaceous carbonates (Cantabria, northern Spain): Results of petrographic, geochemical and petrophysical studies, Bull. Soc. Géol. Fr. 181(49), 391-407.
- Sharp, I., Gillespie, P., Morsalnezhad, D., Taberner, C., Karpuz, R., Vergés, J, Horbury, A., Pickard, N., Garland, J., Hunt, D., 2010. Stratigraphic architecture and fracture-controlled dolomitization of the Cretaceous Khami and Bangestan groups: an outcrop case study, Zagros Mountains, Iran., in: van Buchem, F.S.P., Gerdes, K.D., Esteban, M., (Eds.), Mesozoic and Cenozoic Carbonate Systems of the Mediterranean and the Middle East: Stratigraphic and Diagenetic Reference Models, Geol. Soc, Lond. Sp. Publ. 329, London, pp. 343-396.
- Sibley D.F., Nordeng, S.H., Barkowski, M.L., 1994. Dolomitization kinetics in hydrothermal bombs and natural settings. J. Sed. Res. 64A, 630-637.
- Sibley D.F., Gregg, J.M., 1987. Classification of dolomite rock textures. J. Sed. Petrol. 57, 967-975.
- Simón, J.L., 2004. La estructura extensional neógena-cuaternaria en la Cordillera Ibérica, in: Vera, J.A., (Ed.), Geología de Espaa. Sociedad Geológica de Espaa-IGME, Madrid, pp. 615-617.
- Sptl, C., Pitman, J.K., 1998. Saddle (baroque) dolomite in carbonates and sandstones: a reppraisal of the burial-diagenetic concept, in: Morad, S. (Ed.), Carbonate Cementation in Sandstones, International Assoc. Sed. Sp. Pub. 26, pp 437-460.
- Stafford, S., Whitaker, F., Xiao, Y., Gomez-Rivas, E., Martín-Martín, J.D., 2009. Utilizing Reactive Transport Modelling to Inverse Model the Origin and Evolution of Stratiform Dolomite Geobodies and MVT Deposits, Maestrat Basin, Iberian Chain, Spain. AAPG Annual Convention and Exhibition, Book of Abstracts, Denver. Sun, S.Q., Esteban, M., 1994. Paleoclimatic controls on sedimentation, diagenesis, and reservoir quality: Lessons from Miocene carbonates. AAPG Bull. 78, 519-543.
- Swennen, R., Dewit, J., Fierens, E., Muchez, P., Shah, M., Nader, F. H., Hunt, D., 2012. Multiple dolomitisation events along the Pozalagua Fault (Pozalagua Quarry, Basque-Cantabrian Basin, Northern Spain). Sedimentology 59, 13451374.
- Tomás, S., 2007. Sistemas arrecifales del Cretácico inferior de la Cuenca del Maestrat. Modelos deposicionales, paleontológicos y diagenéticos. Unpublished PhD thesis, Universitat de Barcelona, Spain.

- Tomás, S., Comas Nebot, M. and Salas, R., 2007. La plataforma carbonatada Aptiense superior de Benicàssim-Orpesa (Cuenca del Maestrat, Cadena Ibérica): modelo de depósito. Geogaceta 41, 235-238.
- Tomás, S., Lser, H., Salas, R., 2008. Low-light and nutrient-rich coral assemblages in an Upper Aptian carbonate platform of the southern Maestrat Basin (Iberian Chain, eastern Spain). Cret. Res. 29, 509-534.
- Tritlla, J., Cardellach, E., 2003. Hg-Ba deposits in the Espadà (Iberian Chain, eastern Spain): an example of Cretaceous fluid circulation and Alpine overprinting. J. Geoch. Expl. 78-79, 579-584.
- Tritlla, J., Solé, J., 1999. A newly dated Cretaceous hydrothermal event in the Iberian Ranges, (Eastern Spain) and its significance within the Mesozoic thermal history in the Iberian Peninsula. Ore Geol. Rev. 15, 243-259.
- Wardlaw, N.C., 1976. Pore Geometry of Carbonate Rocks as Revealed by Pore Casts and Capillary Pressure. AAPG Bull. 60(2), 245-257.
- Warren, J., 2000. Dolomite: occurrence, evolution and economically important associations. Earth-Sci. Rev. 52, 1-81.
- Warren, J.K., 2006. Evaporites. Sediments, Resources and Hydrocarbons. Springer. Berlin.
- Whitaker, F.F., Smart, P.L., Jones, G.D., 2004. Dolomitization: From conceptual to numerical models, in: Braithwaite, C.J.R., Rizzi, G., Darke, G., (Eds.), The Geometry and Petrogenesis of Dolomite Hydrocarbon Reservoirs. Geol. Soc. Lond. Sp. Pub. 235, London, pp. 99-139.
- Wilson, M.I.J., Evans, M.J., Oxtoby, N.H, Nas, D.S. Donnelly, T., Thirwall, M., 2007. Reservoir quality, textural evolution, and origin of fault-associated dolomites. AAPG Bull. 91(9), 1247-1272.
- Wilson, A.M., Sanford, W.E., Whitaker, F.A., Smart, P.L., 2001. Spatial patterns of diagenesis during geothermal circulation in carbonate platforms. Am. J. Sci. 301, 727-752.